

Hierarchical Sparse Bayesian Multitask Model with Scalable Inference for Microbiome Analysis

Haonan Zhu^{1,2,*}, Andre R. Goncalves^{1,*}, Camilo Valdes¹, Hiranmayi Ranganathan¹, Boya Zhang¹, Jose Manuel Marti¹, Car Reen Kok¹, Monica K. Borucki¹, Nisha J. Mulakken¹, James B. Thissen¹, Crystal Jaing¹, Alfred Hero², and Nicholas A. Be^{1,*}

¹Lawrence Livermore National Laboratory

²Electrical and Computer Engineering, University of Michigan

*Corresponding Authors: zhu18@llnl.gov, andre@llnl.gov, be1@llnl.gov

Abstract—This paper proposes a hierarchical Bayesian multitask learning model that is applicable to the general multitask binary classification learning problem where the model assumes a shared sparsity structure across different tasks. We derive a computationally efficient inference algorithm based on variational inference to approximate the posterior distribution. We demonstrate the potential of the new approach on various synthetic datasets and for predicting human health status based on microbiome profile. Our analysis incorporates data pooled from multiple microbiome studies, along with a comprehensive comparison with other benchmark methods. Results in synthetic datasets show that the proposed approach has superior support recovery property when the underlying regression coefficients share a common sparsity structure across different tasks. Our experiments on microbiome classification demonstrate the utility of the method in extracting informative taxa while providing well-calibrated predictions with uncertainty quantification and achieving competitive performance in terms of prediction metrics. Notably, despite the heterogeneity of the pooled datasets (e.g., different experimental objectives, laboratory setups, sequencing equipment, patient demographics), our method delivers robust results.¹

Index Terms—Bayesian Hierarchical Model, Multitask Learning, Human Microbiome, Disease Prediction, Variational Inference.

I. INTRODUCTION

Multitask learning (MTL) is a class of machine learning prediction models where multiple related learning tasks are trained jointly [1] (see [2] for a recent survey). This allows us to combine multiple related tasks (datasets, for example) together to increase the effective sample size, while keeping the interpretability of a single base model. MTL has been an active area of research with applications including: face recognition in computer vision; joint analysis of heterogeneous genomics data; social media sentiment analysis; and climate sciences [3], [4], [5], [6], [7].

¹This work was performed under the auspices of the U.S. Department of Energy by Lawrence Livermore National Laboratory under Contract DE-AC52-07NA27344 (LLNL-MI-853606). It was supported by the LLNL Laboratory Directed Research and Development Program, the ETI Consortium under US Department of Energy grant DE-NA0003921, and the US Army Research Office under grant number W911NF1910269.

In this paper, we introduce a hierarchical sparse Bayesian multitask logistic regression model tailored for binary predictions on multiple related datasets. While the model is broadly applicable, we focus on the predictions of a binary health or disease state across multiple possible disease conditions of patients based on microbiome abundance data.

The human microbiome, composed of all the microorganisms associated with the human body, have an immense impact on human health. An abundance of studies demonstrate the promise of microbiome features as indicators of human health outcomes, including in gastrointestinal (GI) health [8], [9], [10], [11], [12], cancer [13], [14], [15], neurological disease [16], [10], and immune dysfunction [11], [12]. Motivated by the success of machine learning models in areas such as computer vision, medical imaging, and protein prediction [17], [18], [19], there has been an increasing interest in employing machine learning models to perform health prediction based on human gut microbiome data [20], [21], [22], [23]. However, application of machine learning methods to microbiome data faces two major challenges. First, typical microbiome data, potentially representative of thousands of species, is high dimensional, and the number of microbial identifiers is significantly larger than the number of samples available for any given study [20]. In this regime, overparameterized models can easily overfit to the training data [24]. Second, in health applications it is essential that machine learning models be interpretable and quantify uncertainty in their predictions, which is not the case with most deep neural nets [25]. In general, clinical and other critical applications benefit from known uncertainty in the predictions of an interpretable model [26].

We propose an interpretable predictive model that is based on a hierarchical Bayesian generalized linear model (GLM) [27]. The model introduces a set of binary variables shared across different datasets to represent the most informative features (i.e., microbial taxonomic identifiers) for predictions. This enables the model to identify the common microbial species shared across the different studies, and to determine which species correspond to a distinct given pathology.

In contrast to optimization based MTL approaches [28], [29], [7], [30], our proposed Bayesian hierarchical modeling provides natural uncertainty quantification through the posterior

distribution of the label given the features and provides a flexible framework to incorporate domain experts’ knowledge [31]. The proposed model differs from [32], [33], [28], [29], [30], [34] in how the sparsity pattern is modeled: inspired by [34] we use an overparameterized Bernoulli-Gaussian model instead of regularizations, which has been demonstrated to have better support recovery properties [35]. The Bayes posterior distribution is not in analytical closed form and we propose an approximation to the posterior mode that is based on variational inference [36], [37], which is more scalable to the high dimensional microbiome datasets.

We illustrate our model capabilities through numerical experiments in simulated data and in a real world microbiome dataset. This dataset is composed of 61 different previously published studies, which were internally curated and the raw sequence data processed for metagenomic classification and sequence-read abundance estimation [38]. See section I of supplementary materials for a full description and the list of references. Each study from the data performed an assessment of a patient cohort’s gut or fecal microbiota in the context of the health condition of the patients, which was assigned a binary label of *control* or *diseased*.

To generate microbiome profiles that are consistent across studies, all raw DNA sequence data was re-processed the same way. DNA sequence data were downloaded from the appropriate repository corresponding to each study referenced above. All sequence datasets were composed of short-read data generated via an Illumina sequencer platform. DNA sequence was quality filtered via fastp [39]. Metagenomic classification and taxonomic assignment of all sequence reads was performed via Centrifuge [40], [41] employing a reference index database constructed from sequences contained in the NCBI Nucleotide (nt) database [42] of December 13, 2021. Post-processing and filtering using a Minimum Hit Length of 40 was performed via Recentrifuge [43]. The resultant output consists of sequence read counts that were assigned to each observed taxonomic identifier (taxID) in the reference index.

Resultant read count values for each taxonomic identifier were further processed by centered log ratio (CLR) transform [44] to provide features for the machine learning model. Seven total taxonomic rank levels were examined for purposes of this analysis, and we take the union set of all the taxIDs for each taxonomic rank to provide a consistent feature space. The taxonomic ranks are: Kingdom (11), Phylum (160), Class (313), Order (868), Family (2338), Genus (7519) and Species (31679), where each number in the parentheses corresponds to the feature dimension (i.e., total number of taxIDs). The health condition studied for each patient is one-hot coded into one of the 19 conditions examined in the selected dataset: cirrhosis, inflammatory bowel disease, diabetes, diarrhea, cancer, dermatologic disease, oral disease, cardiovascular disease, neurological disease, gastrointestinal infection, autoimmune disease, genitourinary disease, pulmonary disease, aged-related macular degeneration, hormonal disorder, immune disease, metabolic disease, seafaring syndrome and irritable bowel syndrome. Each distinct disease condition contains one or

more studies, and we map the studies of the same disease into different tasks, while modeling each disease as a separate multitask-learning model. The resulting model is a direct clustering extension of the proposed Bayesian hierarchical model.

The proposed model is evaluated in comparison with other benchmark methods including: logistic regression with sparsity penalty [45], [46], MTFL (Multitask Feature Learning) [28] and MSSL (Multitask Sparsity Structure Learning) [7]. Our evaluation with simulated synthetic datasets shows that the proposed approach has superior support recovery properties when the underlying regression coefficients share a common sparsity structure across different tasks. The proposed model performs less robustly on the real microbiome data, likely due to heterogeneity of the datasets (different experimental objectives, laboratory protocols, sequencing instrumentation, patient demographics etc.), Nonetheless, we demonstrate the utility of the method to extract informative taxa while providing well-calibrated predictions with uncertainty quantification.

The paper is organized as follows: Section II introduces the mathematical formulation of the proposed hierarchical Bayesian model, Section III presents the proposed variational inference algorithm to obtain the approximated posterior distribution, Section IV provides application of the methods to synthetic datasets and the microbiome dataset, and Section V summarizes the findings from the paper and discusses future directions.

II. HIERARCHICAL SPARSE BAYESIAN MULTITASK LOGISTIC REGRESSION MODEL

A. Notations and Terminologies

We refer to the abundance of each taxonomic identifier (taxID) as a feature variable. Each study is referred to as a task, and diseased or healthy state of the individual is referred to as a label. We use bold upper-case letters for matrices, bold lower case letters for vectors and no bold lower case for scalars. The Hadamard (element-wise) product of vectors \mathbf{a} and \mathbf{b} is denoted by $\mathbf{a} \circ \mathbf{b}$, and diag denotes the function map a vector to a diagonal matrix with the vector as its diagonal entries. We denote the observed taxID count data after centered log ratio transform as $\mathbf{x}_t^i \in \mathbb{R}^d$ together with its label $y_t^i \in \{0, 1\}$, where d corresponds to the number of features (i.e., number of taxIDs), $t = 1, \dots, T$ denotes the different tasks (i.e., different studies), $i = 1, \dots, n_t$ denotes the different subjects per study, n_t denotes the total number of subjects per task, and y_t^i reflect whether the subject is diseased (1) or control (0). For a given regression weight matrix $\mathbf{W} \in \mathbb{R}^{T \times d}$ for all the tasks, we denote $\mathbf{w}_t \in \mathbb{R}^d$ the row vector of \mathbf{W} corresponds to t -th task across features, and $\mathbf{w}_{(j)} \in \mathbb{R}^T$ the column vector of \mathbf{W} corresponds to j -th feature across tasks.

B. Hierarchy Bayesian Multitask Logistic Regression Model

Though the number of microbial species are on the order of trillions on earth, a much smaller quantity of species are capable of causing disease in humans [47]. Our model therefore assumes that only a few of the microbial species are useful for the prediction task, where we impose sparsity on the regression coefficient through a Bernoulli-Gaussian distribution ($\mathbf{w}_t \circ \mathbf{z}$)

[48], [35], where \mathbf{w}_t controls the magnitude of the effects and \mathbf{z} controls the sparsity. This compound prior enforces some of the weights to be exactly zero, implying some of the microbial species are irrelevant for predicting the health status of any given subject. The sparsity term \mathbf{z} is independently drawn from the same Bernoulli distribution with parameter θ . Note \mathbf{z} does not depend on the specific task. This implies the sparsity pattern is shared across different tasks, which reflects the belief that there are few microbial species useful for prediction across all tasks relative to the total quantity of microbial taxa contained in the datasets. A hyper prior for θ is given by the beta distribution, which utilizes the conjugate property to control the overall sparsity level of the model. Further, to enforce the information sharing across different tasks, the row of \mathbf{W} , denoted by $\mathbf{w}_{(j)}$ are assumed to be *i.i.d* draws from a multivariate Gaussian distribution with mean $\mathbf{0}$ and covariance Σ_0 . A Wishart prior is proposed for this shared covariance matrix to provide a method for utilizing expert knowledge about the underlying relationships among the studies. This enables us to exploit the Wishart-normal conjugacy to obtain efficient inference later. The proposed conditional model can be summarized:

$$\begin{aligned} y_t^i | \mathbf{w}_t, \mathbf{z}; \mathbf{x}_t^i &\overset{\text{independent}}{\sim} \text{Bernoulli} \left(\text{sigmoid} \left(\langle (\mathbf{w}_t \circ \mathbf{z}), \mathbf{x}_t^i \rangle \right) \right) \\ &\quad \forall i = 1, \dots, n_t, \forall t = 1, \dots, T, \\ z_j | \theta &\overset{\text{i.i.d}}{\sim} \text{Bernoulli}(\theta) \quad \forall j = 1, \dots, d, \\ \theta &\sim \text{Beta}(\alpha_0, \beta_0), \\ \mathbf{w}_{(j)} | \Sigma_0 &\overset{\text{i.i.d}}{\sim} \mathcal{N}(\mathbf{0}, \Sigma_0) \quad \forall j = 1, \dots, d, \\ \Sigma_0^{-1} &\sim \text{Wishart}(v_0, \mathbf{V}_0). \end{aligned}$$

where $\alpha_0, \beta_0, v_0, \mathbf{V}_0$ are hyperparameters selected by the experimenter. Smaller value of the ratio $\frac{\alpha_0}{\alpha_0 + \beta_0}$ corresponds to a prior belief of fewer informative features while the magnitude α_0 controls the confidence of prior belief, and v_0, \mathbf{V}_0 reflects the prior knowledge about the covariance structure of the regression coefficient \mathbf{W} across different tasks. See Fig. 1 for a visualization of the proposed model and its cluster extension used in subsection IV-B.

The proposed model leads to a log conditional probability, up to an unimportant constant:

$$\begin{aligned} &\log(p(\mathbf{Y}, \mathbf{W}, \Sigma_0, \theta | \mathbf{X}; v_0, \mathbf{V}_0, \alpha_0, \beta_0)) \\ &= -\frac{1}{2} \text{tr}(\mathbf{V}_0^{-1} \Sigma_0^{-1}) \\ &\quad + \frac{v_0 + d - T - 1}{2} \log \det(\Sigma_0^{-1}) \\ &\quad - \frac{v_0}{2} \log \det(\mathbf{V}_0) \\ &\quad + (\alpha_0 - 1) \log(\theta) + (\beta_0 - 1) \log(1 - \theta) \\ &\quad + \log \Gamma(\alpha_0 + \beta_0) - \log \Gamma(\alpha_0) - \log \Gamma(\beta_0) \\ &\quad - \sum_j \frac{1}{2} \langle \mathbf{w}_{(j)}, \Sigma_0^{-1} \mathbf{w}_{(j)} \rangle \\ &\quad + \sum_t \sum_i y_t^i \left(\langle (\mathbf{w}_t \circ \mathbf{z}), \mathbf{x}_t^i \rangle \right) \\ &\quad - \sum_t \sum_i \log \left(\exp \left(\langle (\mathbf{w}_t \circ \mathbf{z}), \mathbf{x}_t^i \rangle \right) + 1 \right) \\ &\quad + \left(\sum_j z_j \right) \log \theta + \left(d - \sum_j z_j \right) \log(1 - \theta). \quad (1) \end{aligned}$$

where Γ denotes the gamma function.

III. VARIATIONAL INFERENCE

With the combination of the logistic function and the hierarchical structure, inference from the exact posterior distribution of the conditional model is intractable since the posterior distribution is not available in closed form. We resort to a variational approach [36], [37] where we approximate the posterior distribution with a simpler distribution, and the approximation is iteratively refined. We refer interested readers to [36] for a comprehensive review on variational inference (VI) as a general approach for Bayesian inference.

Section III-A introduces the mean-field approximation used to approximate the posterior distribution along with the variational objective function, and Section III-B summarizes the optimization algorithm based on coordinate ascent [49].

A. Mean-Field Approximation and Variational Lower Bound

Mean field approximation is a commonly used approximation because it is expressive enough to approximate the complex posteriors, and yet simple enough to lead to tractable computations [49].

In this work, we propose to approximate the true posterior of the proposed model by the function:

$$q(\theta, \mathbf{W}, \Sigma_0, \mathbf{z}) = q(\theta; \alpha, \beta) q(\Sigma_0^{-1}; v, \mathbf{V}) \prod_j q(z_j; \phi_j) q(\mathbf{w}_{(j)}; \mathbf{m}_{(j)}, \Sigma_j). \quad (2)$$

where $q(\theta; \alpha, \beta)$ is a beta distribution with parameters (α, β) , $q(z_j; \phi_j)$ is a Bernoulli distribution with parameters ϕ_j , $q(\Sigma_0^{-1}; v, \mathbf{V})$ is a Wishart distribution with parameters (v, \mathbf{V}) , and $q(\mathbf{w}_{(j)}; \mathbf{m}_{(j)}, \Sigma_j)$ is a multivariate Gaussian distribution with mean $\mathbf{m}_{(j)}$ and covariance Σ_j for $j = 1, \dots, d$.

The optimization objective of variational inference (VI) is to minimize the KL-divergence between the approximation Eqn. 2 and the true posterior by maximizing the evidence lower bound (ELBO):

$$\begin{aligned} \text{ELBO}(q) &= \mathbb{E}_q[\log f(\mathbf{X}, \mathbf{Y}, \theta, \mathbf{z}, \mathbf{W}, \Sigma_0)] + \text{Entropy}(q) \\ &= -\frac{1}{2} \text{tr}(v \mathbf{V}_0^{-1} \mathbf{V}) + \frac{v_0 + d}{2} \log \det(\mathbf{V}) \\ &\quad + \frac{v_0 + d - v}{2} \psi_T \left(\frac{v}{2} \right) + \frac{vT}{2} + \ln \Gamma_T \left(\frac{v}{2} \right) \\ &\quad + \left(\alpha_0 + \sum_j \phi_j - \alpha \right) \psi(\alpha) + \ln B(\alpha, \beta) \\ &\quad + \left(\beta_0 + d - \sum_j \phi_j - \beta \right) \psi(\beta) \\ &\quad + (\alpha + \beta - d - \alpha_0 - \beta_0) \psi(\alpha + \beta) \\ &\quad - \frac{1}{2} \sum_j \text{tr}(v \mathbf{V}(\mathbf{m}_{(j)} \mathbf{m}_{(j)}^\top + \Sigma_j)) \\ &\quad + \sum_t \sum_i y_t^i \left(\langle (\mathbf{m}_t \circ \phi), \mathbf{x}_t^i \rangle \right) \\ &\quad - \sum_t \sum_i \mathbb{E}_{\mathbf{W}, \mathbf{z} \sim q} \left[\log \left(\exp \left(\langle (\mathbf{w}_t \circ \mathbf{z}), \mathbf{x}_t^i \rangle \right) + 1 \right) \right] \\ &\quad + \frac{1}{2} \sum_j \log \det(\Sigma_j) - \sum_j \phi_j \log(\phi_j) \\ &\quad - \sum_j (1 - \phi_j) \log(1 - \phi_j). \quad (3) \end{aligned}$$

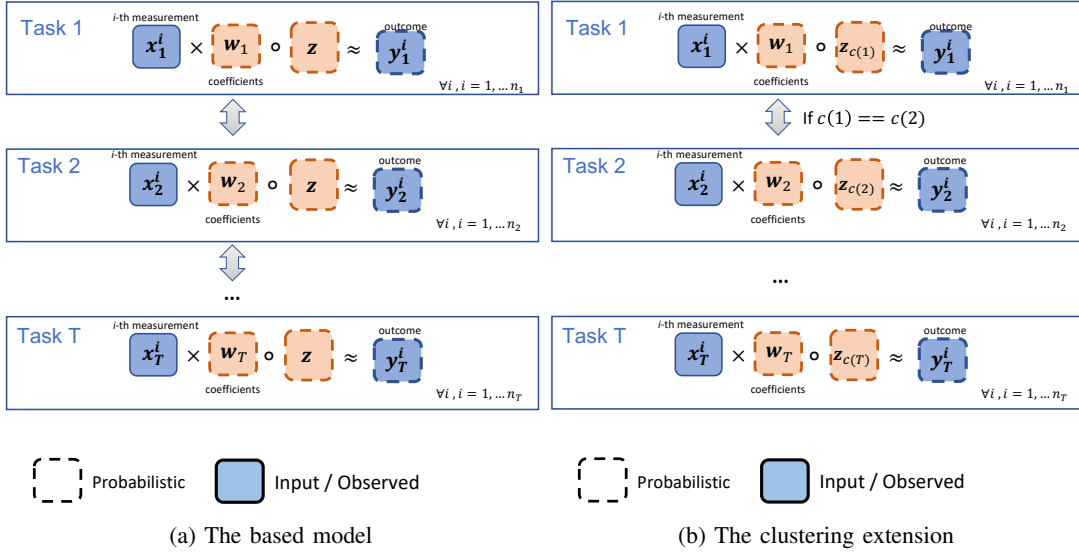


Fig. 1: Graphical visualization of the proposed probabilistic model. For the base model in (a), the information sharing cross different tasks is enforced by common priors between the regression weights and sparsity parameters. For the clustering extension (b), the information sharing is limited to tasks from the same cluster (i.e., disease category).

where ψ is the digamma function, ψ_T is the multivariate digamma function and γ_T is the multivariate gamma function. Since the expectations of the sigmoid functions do not admit closed form solutions, we approximate the sigmoid functions by quadratic lower bounds:

$$\begin{aligned}
& -\log \left(\exp \left(\langle (\mathbf{w}_t \circ \mathbf{z}), \mathbf{x}_t^i \rangle \right) + 1 \right) \\
& \geq -\log \left(\exp \left(\langle (\mathbf{w}'_t \circ \mathbf{z}'), \mathbf{x}_t^i \rangle \right) + 1 \right) \\
& \quad - \frac{\langle \mathbf{x}_t^i, \mathbf{w}_t \circ \mathbf{z} - \mathbf{w}'_t \circ \mathbf{z}' \rangle}{\exp \left(\langle (\mathbf{w}'_t \circ \mathbf{z}'), \mathbf{x}_t^i \rangle \right) + 1} \\
& \quad - \frac{1}{8} (\mathbf{w}_t \circ \mathbf{z} - \mathbf{w}'_t \circ \mathbf{z}')^\top \mathbf{x}_t^i \left(\mathbf{x}_t^i \right)^\top (\mathbf{w}_t \circ \mathbf{z} - \mathbf{w}'_t \circ \mathbf{z}'). \quad (4)
\end{aligned}$$

for $i = 1, \dots, n_t, t = 1, \dots, T$, and $\mathbf{w}'_t, \mathbf{z}'$ are deterministic reference points of choice. This type of approximations has been used to design majorize-minimization (MM) algorithms for the logistic regression problem [50], [51]. The resulting approximation is, up to a constant:

$$\begin{aligned}
& -\sum_t \sum_i \mathbb{E}_{\mathbf{w}, \mathbf{z} \sim q} \left[\log \left(\exp \left(\langle (\mathbf{w}_t \circ \mathbf{z}), \mathbf{x}_t^i \rangle \right) + 1 \right) \right] \\
& \geq -\sum_t \sum_i \log \left(\exp \left(\langle (\mathbf{w}'_t \circ \mathbf{z}'), \mathbf{x}_t^i \rangle \right) + 1 \right) \\
& \quad + \sum_t \sum_i \frac{\langle \mathbf{w}'_t \circ \mathbf{z}', \mathbf{x}_t^i \rangle}{\exp \left(-\langle (\mathbf{w}'_t \circ \mathbf{z}'), \mathbf{x}_t^i \rangle \right) + 1} \\
& \quad - \frac{1}{8} \sum_t \sum_i \langle \mathbf{w}'_t \circ \mathbf{z}', \mathbf{x}_t^i \rangle^2 \\
& \quad - \sum_t \sum_i \frac{1}{\exp \left(-\langle (\mathbf{w}'_t \circ \mathbf{z}'), \mathbf{x}_t^i \rangle \right) + 1} \langle \mathbf{x}_t^i, (\mathbf{m}_t \circ \phi) \rangle \\
& \quad + \frac{1}{4} \sum_t \sum_i \langle \mathbf{w}'_t \circ \mathbf{z}', \mathbf{x}_t^i \rangle \langle \mathbf{m}_t \circ \phi, \mathbf{x}_t^i \rangle \\
& \quad - \frac{1}{8} \sum_t \sum_i \langle \mathbf{m}_t \circ \phi, \mathbf{x}_t^i \rangle^2 \\
& \quad + \frac{1}{8} \sum_t \sum_j (\mathbf{m}_{t,j}^2 (\phi_j - 1) - (\Sigma_j)_{t,t}) \phi_j \sum_i (\mathbf{x}_t^{ij})^2. \quad (5)
\end{aligned}$$

There are other alternative approaches using different lower bounds [52], [53], chapter 10.6 of [49], but they require additional variational parameters that scale with the feature dimension (d), which complicates the variational computations.

B. Coordinate Ascent Variational Inference (CAVI)

Coordinate ascent variational inference (CAVI) [49] is a optimization technique where we optimize one set of the variational parameters at a time while holding the others fixed.

One useful result (Equation 18 of [36]) states that if we are to approximate a general posterior distribution $p(\boldsymbol{\xi} \mid \text{data})$ with a mean-field approximation $q(\boldsymbol{\xi}) := \prod_j q_j(\xi_j)$, the CAVI update for j -th latent variable ξ_j (i.e., the optimal solution $q_j^*(\xi_j)$) is proportional to the exponentiated conditional expected log of the joint:

$$q_j^* \propto \exp \left(\mathbb{E}_{\boldsymbol{\xi}_{-j} \sim q_{-j}} \left[\log \left(p(\xi_j, \boldsymbol{\xi}_{-j} \mid \text{data}) \right) \right] \right). \quad (6)$$

where $\boldsymbol{\xi}_{-j}$ corresponds to all but the j -th latent variable.

The resulting Coordinate Ascent Variational Inference (CAVI) algorithm is summarized in Algorithm. 1, and see section II of supplementary materials for details of the derivations.

IV. EXPERIMENTS

In this section, we evaluate the performance of our proposed method on both simulated data and real microbiome data pooled from multiple studies (see section I of supplementary materials for a full description and the list of references), and we compare it with following methods:

- Single-task Logistic Classifier with sparsity penalty (STL-LC) [45], [46]: this is a single-task model, where we fit independent logistic models to each task separately. This is an extension of standard LASSO to the binary classification setting.

Algorithm 1 CAVI for Bayesian Multitask Sparse Logistic Regression

```

1: procedure CAVI(Inputs:  $(\mathbf{x}_t^i, y_t^i)_{t=1, \dots, T, i=1, \dots, n_t}$ )
2:   for all itr = 1, ..., Niter do
3:     for all  $j = 1, \dots, d$  do
4:        $\tilde{\mathbf{X}}_j \leftarrow \text{diag} \left( \begin{bmatrix} \sum_i \phi_j(x_1^{ij})^2 \\ \vdots \\ \sum_i \phi_j(x_T^{ij})^2 \end{bmatrix} \right)$ 
5:        $\Sigma_j \leftarrow (v\mathbf{V} + \frac{1}{4}\tilde{\mathbf{X}}_j)^{-1}$ 
6:       end for
7:       for all  $j = 1, \dots, d$  do
8:         for all  $t = 1, \dots, T, i = 1, \dots, n_t$  do
9:            $\tilde{y}_t^i \leftarrow \text{sigmoid} \left( \sum_j m_{tj} x_t^{ij} \phi_j \right)$ 
10:        end for
11:         $\mathbf{m}_{(j)} \leftarrow \Sigma_j \begin{bmatrix} \phi_j \sum_i (y_1^i - \tilde{y}_1^i) x_1^{ij} \\ \vdots \\ \phi_j \sum_i (y_T^i - \tilde{y}_T^i) x_T^{ij} \end{bmatrix}$ 
12:         $+ \frac{1}{4}\Sigma_j \begin{bmatrix} \phi_j^2 \sum_i (x_1^{ij})^2 m_{1j} \\ \vdots \\ \phi_j^2 \sum_i (x_T^{ij})^2 m_{Tj} \end{bmatrix}$ 
13:        end for
14:        for all  $j = 1, \dots, d$  do
15:          for all  $t = 1, \dots, T, i = 1, \dots, n_t$  do
16:             $\tilde{y}_t^i \leftarrow \text{sigmoid} \left( \sum_j m_{tj} x_t^{ij} \phi_j \right)$ 
17:          end for
18:           $\phi_j \leftarrow \text{sigmoid} \left( \psi(\alpha) - \psi(\beta) \right)$ 
19:           $+ \sum_t \sum_i (y_t^i - \tilde{y}_t^i) m_{tj} x_t^{ij}$ 
20:           $+ \frac{1}{4} \sum_t (m_{tj}^2 \phi_j) \sum_i (x_t^{ij})^2$ 
21:           $- \frac{1}{8} \sum_t m_{tj}^2 \sum_i (x_t^{ij})^2$ 
22:           $- \frac{1}{8} \sum_t (\Sigma_j)_{tt} \sum_i (x_t^{ij})^2$ 
23:        end for
24:         $\alpha \leftarrow \alpha_0 + \sum_j \phi_j,$ 
25:         $\beta \leftarrow \beta_0 + d - \sum_j \phi_j,$ 
26:         $\theta \leftarrow \frac{\alpha}{\alpha + \beta},$ 
27:         $v \leftarrow v_0 + d,$ 
28:         $\mathbf{V} \leftarrow \left( \mathbf{V}_0^{-1} + \sum_j \mathbf{m}_{(j)} \mathbf{m}_{(j)}^\top + \Sigma_j \right)^{-1}$ 
29:      end for
30: end procedure

```

- Pooled Logistic Classifier with sparsity penalty (Pooled-LC): we train a single logistic regression model on the combined data from all datasets.
- MTLF (Multitask Feature Learning) [28]: this is an optimization based approach to multitask learning based on $\ell_{2,1}$ -norm regularization. The proposed method can be seen as a Bayesian Hierarchical extension, and the difference in modeling is manifested in how the sparsity pattern is encouraged: we use an overparameterized Bernoulli-Gaussian model, which has better support re-

covery properties [35].

- MSSL (Multitask Sparse Structure Learning) [7]: this is an optimization based multitask learning approach, where the imposed sparsity structure is on the precision (inverse covariance matrix) of the regression coefficients across tasks. The optimization problem of this formulation is equivalent to the graphical lasso problem [54], [55] for covariance estimation.

a) *Model Selection*: For all the methods, we employ a model selection strategy based on cross-entropy loss on the validation dataset to select the hyperparameters (e.g., $\alpha_0, \beta_0, v_0, \mathbf{V}_0$ of the proposed Bayesian approach). Specifically, we use 10 repeated runs of stratified cross-validation [56] since we have a limited number of samples, and the corresponding class labels are imbalanced.

b) *Evaluation Metric*: the microbiome studies employed for this work have imbalanced class labels. We therefore use balanced accuracy to evaluate the predictive models.

A. Synthetic Datasets

We generate synthetic datasets to examine whether our algorithm is able to: 1) recover the support of the regression coefficients that correspond to informative features for the prediction, which are evaluated by balanced accuracy; 2) recover the ground truth regression coefficients (up to normalization), which are evaluated by cosine distance (i.e., one minus the normalized inner product).

To investigate different data scenarios, we generate six datasets with varying sparsity levels (the common support of regression coefficients across tasks) and class imbalance (whether sample sizes across different tasks are of the same magnitude). Additional details of each dataset are summarized in Table I.

Support Recovery: We evaluate the support recovery of the algorithms by turning the support recovery problem into a binary prediction problem. The result is summarized in Fig. 2. The proposed Bayesian method is the best performing algorithm in most of the metrics across all settings. In particular, when the ground truth regression coefficients have a sparse support, the proposed method achieves near-perfect recovery.

Weight Recovery: We evaluate the prediction performance of the algorithm by assessing how well the algorithms can recover the ground truth regression coefficients. Since the logistic prediction is scale invariant, we evaluate the results by the cosine distance. The result is summarized in Table II. The proposed Bayesian method is the best performing algorithm in all but the dense case.

B. Microbiome Data

In this subsection, we demonstrate a real world application of the proposed model on previously published microbiome data discussed in Section I. Our goal is two fold: 1) show that multitask learning on the one-hot coded vector of diseases can perform accurate disease state classification with uncertainty quantification, and 2) identify the microbes that are associated with human diseases of interest.

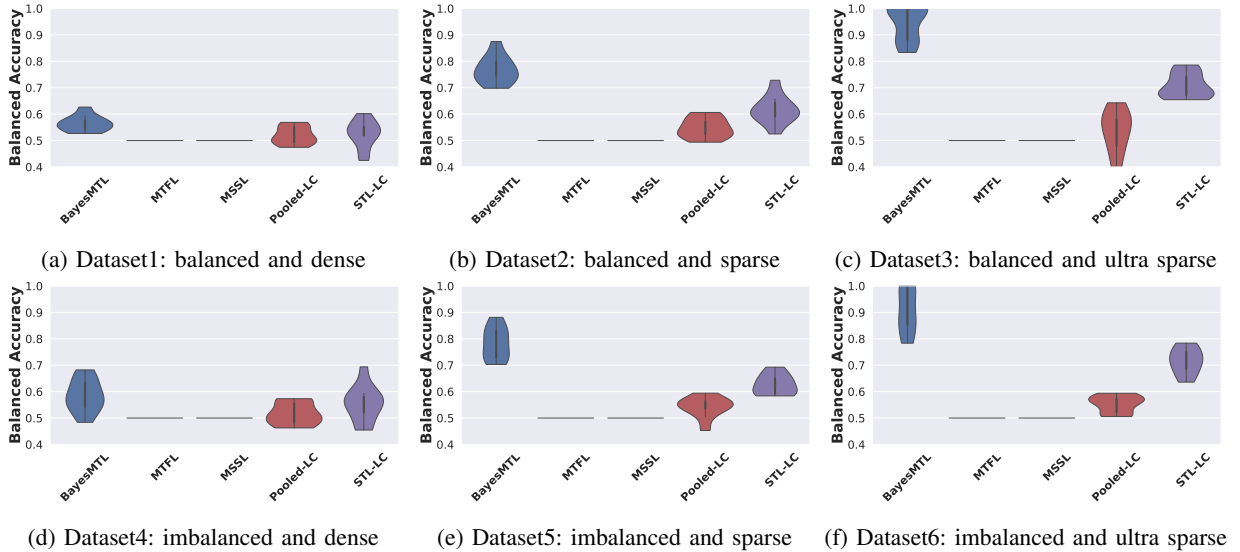


Fig. 2: Summary of the support recovery results for the simulated data evaluated using balanced accuracy across 10 different runs. The proposed Bayesian approach (BayesMTL) outperforms the benchmark methods in terms of balanced accuracy especially when there is a shared sparsity structure across regression coefficients of different tasks. Both MSSL and MTFL prioritize the prediction performance in the cross-validation step which results in complete dense solutions (i.e., all regression coefficients are non-zero), hence they achieve identical accuracy.

	Balanced	Imbalanced
Dense ($\theta = 0.8$)	Dataset-1	Dataset-4
Sparse ($\theta = 0.2$)	Dataset-2	Dataset-5
Ultra Sparse ($\theta = 0.05$)	Dataset-3	Dataset-6

TABLE I: Summary of the simulated dataset, where the sample sizes of balanced data are generated by a Poisson distribution with rate 24, and sample sizes of the imbalanced data are generated by a negative binomial distribution with stopping-time parameter $r = 1$ and probability of success $p = 0.04$. For all the simulations, the number of features is 100 and number of tasks is 10. For the imbalanced datasets, we amplify all the sample sizes by 6 to ensure that both positive samples and negative samples are present across all tasks. Both settings have an expected sample size 30, where the imbalanced case has more variations in sample sizes among different tasks. The θ parameter corresponds to the expected percentage of the predictive features.

	BayesMTL	MTFL	MSSL	STL-LC	Pooled-LC
Dataset-1	0.74 (0.06)	0.56 (0.02)	0.55 (0.02)	0.73 (0.02)	0.98 (0.04)
Dataset-2	0.34 (0.09)	0.56 (0.01)	0.56 (0.01)	0.56 (0.05)	1.02 (0.05)
Dataset-3	0.10 (0.04)	0.59 (0.03)	0.59 (0.02)	0.26 (0.04)	0.99 (0.12)
Dataset-4	0.67 (0.10)	0.58 (0.08)	0.58 (0.05)	0.73 (0.07)	1.02 (0.03)
Dataset-5	0.46 (0.11)	0.59 (0.08)	0.57 (0.04)	1.04 (0.06)	0.57 (0.09)
Dataset-6	0.22 (0.12)	0.65 (0.05)	0.61 (0.04)	0.35 (0.11)	1.07 (0.10)

TABLE II: Summary of the weights recovery measured in cosine distance. The cosine distance is bounded between 0 and 2 with 0 meaning perfect recovery. The proposed Bayesian (BayesMTL) approach outperforms the benchmark methods when there is a shared sparsity structure across regression coefficients of different tasks.

Prediction Performance: analogous to the previous subsection, we evaluate the prediction performance using balanced accuracy, and the result is visualized in Fig. 3. Despite the highly heterogeneous nature of the datasets (i.e., pooled from studies with different experimental objectives, laboratory protocols, sequencing instrumentation, patient demographics etc.), we observe improvements in multitask learning over traditional single-task learning methods for most of the coarser taxonomic ranks, namely Kingdom, Phylum, Class, and Order. This suggests the presence of shareable information across the studies that can be leveraged by the machine learning models. Additionally, our proposed model consistently provides sparse solutions, as evaluated by sparsity ratios (i.e., percentage of the regression coefficients that are zero) as shown in Table III. This aspect is particularly desirable for focusing microbiological analysis of the role of specific microbes in human health.

Taxon Ranks	BayesMTL	MTFL	MSSL	Pooled-LC	STL-LC
Kingdom	0.29 (0.01)	0.54 (0.03)	0.47 (0.03)	0.88 (0.04)	0.26 (0.02)
Phylum	0.18 (0.02)	0.30 (0.002)	0.31 (0.003)	0.78 (0.03)	0.086 (0.02)
Class	0.12 (0.01)	0.24 (0.006)	0.30 (0.05)	0.69 (0.02)	0.070 (0.005)
Order	0.11 (0.01)	0.20 (0.01)	0.22 (0.01)	0.54 (0.009)	0.046 (0.008)
Family	0.043 (0.02)	0.41 (0.3)	0.17 (0.002)	0.41 (0.003)	0.041 (0.007)
Genus	0.018 (0.007)	0.40 (0.3)	0.15 (0.0001)	0.33 (0.003)	0.035 (0.006)
Species	0.029 (0.005)	0.15 (0.03)	0.15 (0.0008)	0.28 (0.004)	0.032 (0.005)

TABLE III: Summary of the results for sparsity ratios (percentage of regression coefficients that are zero). The bold number indicates that the corresponding method gives the sparsest result for the given taxonomic rank, and the values in parentheses represent standard deviations computed over 5 different runs. The proposed approach is the only multitask method that provides a sparse solution, identifying common microbes across studies of the same disease category that are informative for predicting health status.

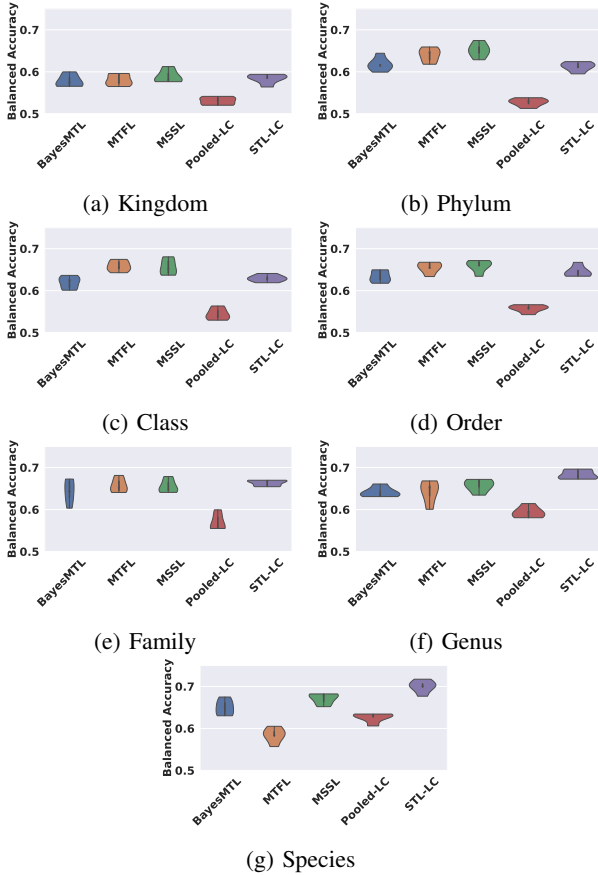
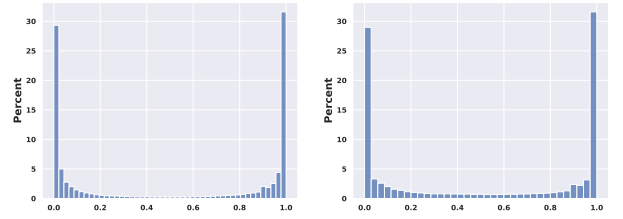


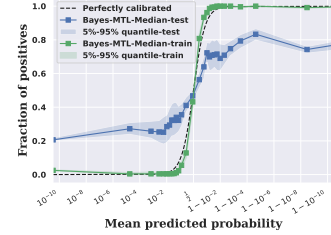
Fig. 3: Summary of the prediction performance evaluated by balanced accuracy across 7 taxonomic ranks. Due to the heterogeneous nature of the data, we do not see an improvement of the proposed approach over single-task models. However, the proposed approach is the only multitask method that provides a sparse solution, i.e., identifying common microbes across studies of the same disease category that are informative for prediction along with uncertainty quantification through the posterior distribution.

Goodness of fit: we evaluate the goodness of fit of the proposed method through calibration curve [57], which plots the predicted probability against the observed labels. For a well calibrated probabilistic model, among all the samples that the model predicted with probability $p\%$ being healthy, close to $p\%$ of them will indeed be healthy. The calibration results are summarized in Fig. 4 for both the training data and test data. The proposed Bayesian approach provides additional uncertainty quantification for the predicted probabilities. Since the proposed model is probabilistic, it provides well calibrated results. The performance degrades at the boundary values for the test data, which indicates that the choice of logit function as a link function is resulting in over-confident predictions. We discuss possible extensions in Section V.

Sparsity visualization: we assign a sparsity coefficient to each of the taxIDs by combining the magnitude of the regression coefficient ($\{w_t\}$) and the sparsity parameters (z). From the estimated posterior distribution, we draw samples



(a) Predicted probabilities on training data. (b) Predicted probabilities on test data.



(c) Calibration curves for the training data and the test data with 90% marginal credible intervals.

Fig. 4: Calibration analysis for the proposed model on the Order taxonomic rank. Fig. (a) and Fig. (b) show the histograms of the predicted probabilities and training and test data respectively. Due to the choice of logit as link function, the predicted probabilities are concentrated around the boundaries. Fig. (c) shows the calibration curves of the predictions from training and test data. The model achieves near perfect calibration on the training data, and the degradation of performance on the test data at the boundary values indicates that the logit function as a link function is resulting in over-confident predictions.

to explore the full distribution of the sparsity coefficient. The most relevant features will correspond to the features with consistent high sparsity coefficients across draws. The result is summarized in Fig. 5. The proposed model learns a sparse set of features shared across different datasets of the same disease from the data as reflected by colored strips. For diabetes and diarrhea, few taxIDs are considered informative for the health prediction task by the model, while for cardiovascular disease, the majority of taxIDs are considered informative.

Feature Selection for Diarrhea Datasets: to further investigate the feature selection capability of the model, we focus on the diarrhea datasets [58], [59], [60] since they have shown consistent sparsity patterns (Fig. 5) and are of particular direct relevance to fecal microbiome and gastrointestinal health. Centered log ratio (CLR) transform is a normalization technique applied to each sample across features, therefore the magnitude of the transformed data varies across features. We propose to assign feature importance of j -th feature (taxID) for task t and sample i by combining the regression coefficient ($\{w_t\}$), the sparsity parameters (z) and the CLR transformed abundance data (x_t^i):

$$\left| \frac{w_{t,j} z_j x_t^{ij}}{\sqrt{\sum_j (w_{t,j} z_j x_t^{ij})^2}} \right|. \quad (7)$$

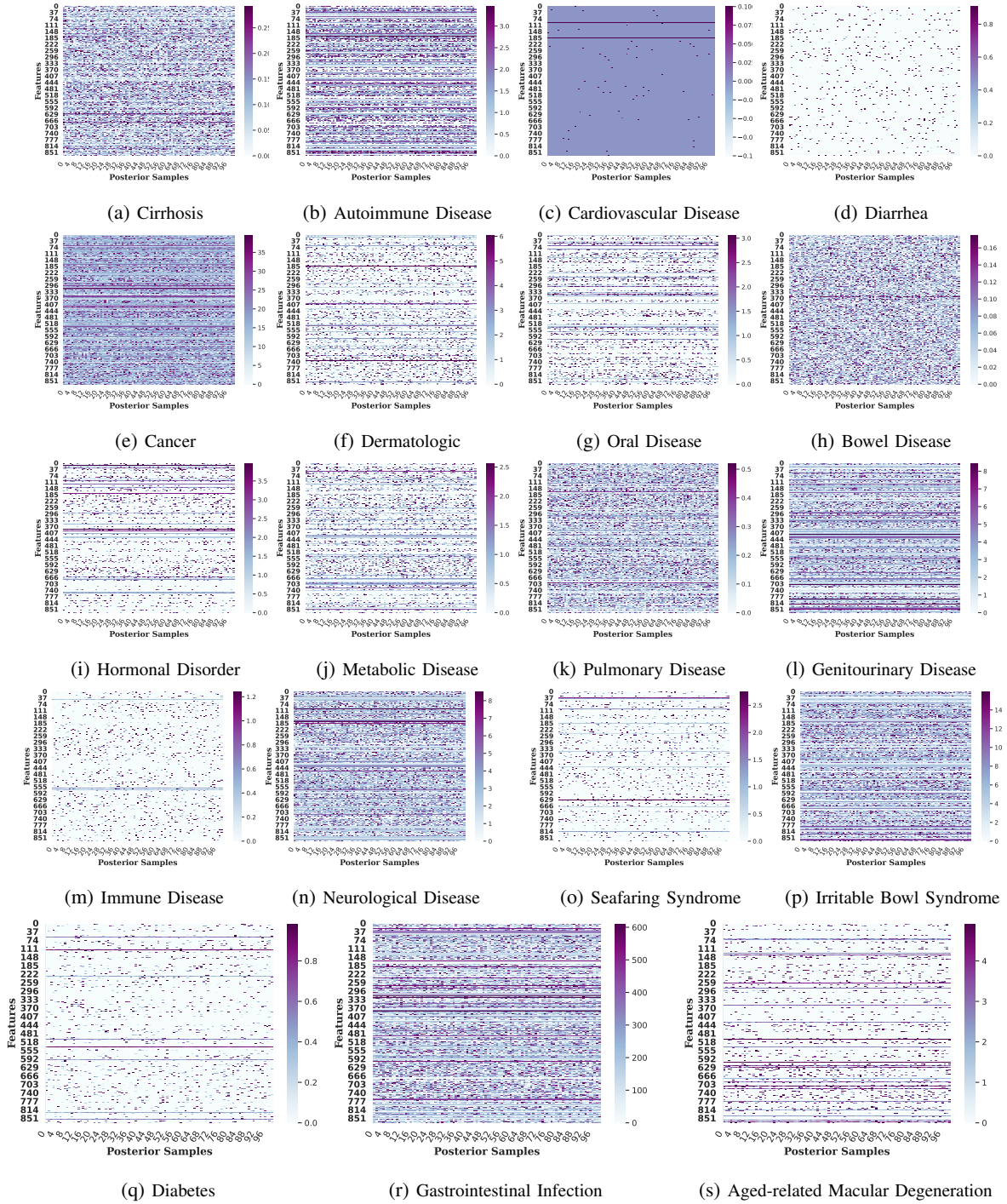


Fig. 5: Feature sparsity visualization across 19 different disease categories of Order taxonomic rank. The x -axis corresponds to different samples drawn from the posterior distribution and the y -axis correspond to different taxIDs. The gradation from white to black for variable color corresponds to its increasing importance weight, and the darker shaded horizontal lines represent the sparse features selected by the algorithm. For diabetes and diarrhea, few taxIDs are considered informative for the health prediction task by the model, while for cardiovascular disease the majority of taxIDs are considered informative.

The proposed importance weight can be interpreted as the relative contribution to the predicted log-odds ratio. From the estimated posterior distribution, we draw samples to explore the full distribution of the feature importance. The most important features will correspond to the features with consistently high importance weights across draws, samples, and tasks. After obtaining important features for each taxonomic rank, we visualize the result using taxonomic lineage information, where lineages with at least 5 taxIDs selected are shown in Fig. 6.

The majority of lineages identified by the model are relevant in the context of the gut microbiome and diet, and highlights the association of *Escherichia coli*, gut bacteriophages (order *Crassvirales*) and a gut fungi, *Debaryomycetaceae* with diarrhea. *Enteroggregative E. coli*, in particular has been routinely discussed to play a causal role in diarrhea [61], [62], [63]. Although our analysis does link *Petitvirales* to healthy controls, these results associate *Crassvirales* with diarrhea (Fig. 6), while previous reports link the abundance of *Crassvirales* with gut health. A number of factors may influence the gut microbiome composition including age, diet, and geographic location [64], [65], [66] thus the datasets used to establish this model may have been influenced by population demographics. Specifically, the diarrhea datasets used here are derived from a mixed population of subjects from Bangladesh and the United States [58], [59], [60]. Additionally, this analysis does not capture other global variables that can contribute to a disease state such as differences in virome richness and diversity [67]. Finally, differences in bioinformatics pipelines and reference databases used to classify sequences likely contributes to reported differences. For example, up to 99% of phage sequences do not map to reference viral genomes [65], [66] thus increasing the likelihood of variability in identification of bacteriophage genomes, which are known for their complex and mosaic genome composition. Furthermore, the identification of plant-related features within the Magnoliopsida class suggest the capability of our approach to identify potentially disease-associated dietary components for hypothesis generation. Bacteriophages belonging to orders *Crassvirales* and *Petitvirales* are highly abundant in the human gut microbiome and have been associated with health [66], [68], [69], [64].

V. CONCLUSION

In this work a hierarchical sparse Bayesian multitask logistic regression model is proposed to predict human health status from human microbiome abundance data. The model is designed to select common informative features across different tasks through the built-in sparsity structure. We derive a computationally efficient inference algorithm based on variational inference. Our simulation studies show that the proposed approach excels in situations when there are shared sparsity structures of the regression coefficients across the different tasks. Our experiments on a real-world dataset pooled from multiple studies demonstrate the utility of the method to extract informative taxa from a large microbiome dataset, while providing well-calibrated predictions with uncertainty quantification.

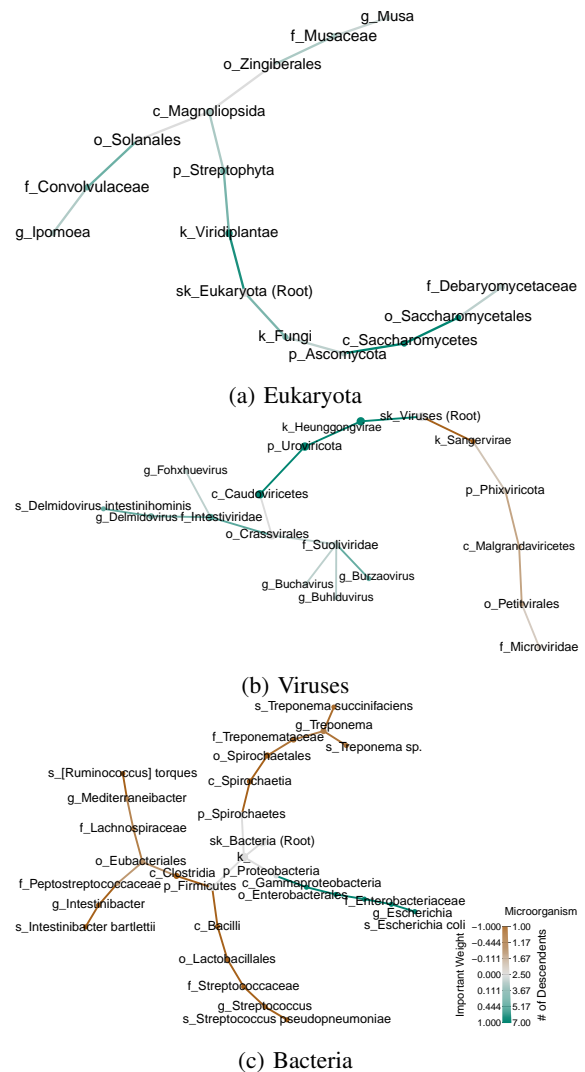


Fig. 6: Lineage analysis of the important features in diarrhea datasets for three distinct taxonomic categories: Eukaryota, Viruses and Bacteria. Each node in the tree corresponds to a taxID. A positive sign (red colored) implies the given taxID is disease associated while a negative sign (green colored) implies the taxID is control associated. The identified lineages include *Escherichia coli* and *Crassvirales* bacteriophages, which have been studied in the context of diarrhea [61], [62], [63], [64].

There are several directions for future work. One direction is to replace the logit function with other link functions (e.g., a probit link function) that have flatter tails so the model is less prone to overconfidence. A second direction is to incorporate additional hierarchical structures into the model that include relevant metadata information such as population demographics. A third direction is to extend our model to multi-label classification problems, where each task contains multiple binary predictions (e.g., diagnosis of different diseases on the same patient). This generalization is of particular interest to the human health prediction application considered in this manuscript, since the diseases are not mutually exclusive. Another related extension is to consider

the multiclass classification problem, where each task is a classification problem with more than 2 labels (e.g., different stages of a disease).

REFERENCES

- [1] Rich Caruana. Multitask learning. *Machine learning*, 28(1):41–75, 1997.
- [2] Yu Zhang and Qiang Yang. A survey on multi-task learning. *IEEE Transactions on Knowledge and Data Engineering*, 2021.
- [3] Xiaogang Wang, Cha Zhang, and Zhengyou Zhang. Boosted multi-task learning for face verification with applications to web image and video search. In *2009 IEEE conference on computer vision and pattern recognition*, pages 142–149. IEEE, 2009.
- [4] Xavier Glorot, Antoine Bordes, and Yoshua Bengio. Domain adaptation for large-scale sentiment classification: A deep learning approach. In *Proceedings of the 28th international conference on machine learning (ICML-11)*, pages 513–520, 2011.
- [5] Christian Widmer and Gunnar Rätsch. Multitask learning in computational biology. In *Proceedings of ICML Workshop on Unsupervised and Transfer Learning*, pages 207–216. JMLR Workshop and Conference Proceedings, 2012.
- [6] Priyadip Ray, Lingling Zheng, Joseph Lucas, and Lawrence Carin. Bayesian joint analysis of heterogeneous genomics data. *Bioinformatics*, 30(10):1370–1376, 2014.
- [7] André R Gonçalves, Fernando J Von Zuben, and Arindam Banerjee. Multi-task sparse structure learning with gaussian copula models. *The Journal of Machine Learning Research*, 17(1):1205–1234, 2016.
- [8] Mirae Lee and Eugene B Chang. Inflammatory bowel diseases (ibd) and the microbiome—searching the crime scene for clues. *Gastroenterology*, 160(2):524–537, 2021.
- [9] Atsushi Nishida, Ryo Inoue, Osamu Inatomi, Shigeki Bamba, Yuji Naito, and Akira Andoh. Gut microbiota in the pathogenesis of inflammatory bowel disease. *Clinical journal of gastroenterology*, 11:1–10, 2018.
- [10] Andrea M McGrattan, Bernadette McGuinness, Michelle C McKinley, Frank Kee, Peter Passmore, Jayne V Woodside, and Claire T McEvoy. Diet and inflammation in cognitive ageing and alzheimer’s disease. *Current nutrition reports*, 8:53–65, 2019.
- [11] F De Luca and Y Shoefeld. The microbiome in autoimmune diseases. *Clinical & Experimental Immunology*, 195(1):74–85, 2019.
- [12] Christoph A Thaiss, Niv Zmora, Maayan Levy, and Eran Elinav. The microbiome and innate immunity. *Nature*, 535(7610):65–74, 2016.
- [13] Sagarika Banerjee, Tian Tian, Zhi Wei, Kristen N Peck, Natalie Shih, Ara A Chalian, Bert W O’Malley, Gregory S Weinstein, Michael D Feldman, James Alwine, et al. Microbial signatures associated with oropharyngeal and oral squamous cell carcinomas. *Scientific reports*, 7(1):4036, 2017.
- [14] Gregory D Sepich-Poore, Laurence Zitvogel, Ravid Straussman, Jeff Hasty, Jennifer A Wargo, and Rob Knight. The microbiome and human cancer. *Science*, 371(6536):eabc4552, 2021.
- [15] Vancheswaran Gopalakrishnan, Beth A Helmink, Christine N Spencer, Alexandre Reuben, and Jennifer A Wargo. The influence of the gut microbiome on cancer, immunity, and cancer immunotherapy. *Cancer cell*, 33(4):570–580, 2018.
- [16] Sarah L Boddy, Ilaria Giovannelli, Matilde Sassani, Johnathan Cooper-Knock, Michael P Snyder, Eran Segal, Eran Elinav, Lynne A Barker, Pamela J Shaw, and Christopher J McDermott. The gut microbiome: a key player in the complexity of amyotrophic lateral sclerosis (als). *BMC medicine*, 19(1):1–14, 2021.
- [17] Kaiming He, Xiangyu Zhang, Shaoqing Ren, and Jian Sun. Delving deep into rectifiers: Surpassing human-level performance on imagenet classification. In *Proceedings of the IEEE international conference on computer vision*, pages 1026–1034, 2015.
- [18] Dinggang Shen, Guorong Wu, and Heung-II Suk. Deep learning in medical image analysis. *Annual review of biomedical engineering*, 19:221, 2017.
- [19] John Jumper, Richard Evans, Alexander Tunyasuvunakool, Tim Green, Michael Figurnov, Olaf Ronneberger, Kathryn Tunyasuvunakool, Russ Bates, Augustin Židek, Anna Potapenko, et al. Highly accurate protein structure prediction with alphafold. *Nature*, 596(7873):583–589, 2021.
- [20] Yi-Hui Zhou and Paul Gallins. A review and tutorial of machine learning methods for microbiome host trait prediction. *Frontiers in genetics*, 10:579, 2019.
- [21] Sachin Aryal, Ahmad Alimadadi, Ishan Manandhar, Bina Joe, and Xi Cheng. Machine learning strategy for gut microbiome-based diagnostic screening of cardiovascular disease. *Hypertension*, 76(5):1555–1562, 2020.
- [22] Giovanni Cammarota, Gianluca Ianiro, Anna Ahern, Carmine Carbone, Andriy Temko, Marcus J Claesson, Antonio Gasbarrini, and Giampaolo Tortora. Gut microbiome, big data and machine learning to promote precision medicine for cancer. *Nature reviews gastroenterology & hepatology*, 17(10):635–648, 2020.
- [23] Ishan Manandhar, Ahmad Alimadadi, Sachin Aryal, Patricia B Munroe, Bina Joe, and Xi Cheng. Gut microbiome-based supervised machine learning for clinical diagnosis of inflammatory bowel diseases. *American Journal of Physiology-Gastrointestinal and Liver Physiology*, 320(3):G328–G337, 2021.
- [24] Ian Goodfellow, Yoshua Bengio, and Aaron Courville. *Deep learning*. MIT press, 2016.
- [25] Christoph Molnar. *Interpretable machine learning*. Lulu. com, 2020.
- [26] Christopher E. Lawson, Jose Manuel Martí, Tijana Radivojevic, Sai Vamshi R. Jonnalagadda, Reinhard Gentz, Nathan J. Hillson, Sean Peisert, Joonhoon Kim, Blake A. Simmons, Christopher J. Petzold, Steven W. Singer, Aindriya Mukhopadhyay, Deepti Tanjore, Joshua G. Dunn, and Hector Garcia Martin. Machine learning for metabolic engineering: A review. *Metabolic Engineering*, 63:34–60, 2021. Tools and Strategies of Metabolic Engineering.
- [27] Annette J Dobson and Adrian G Barnett. *An introduction to generalized linear models*. CRC press, 2018.
- [28] Jun Liu, Shuiwang Ji, and Jieping Ye. Multi-task feature learning via efficient $l_2, 1$ -norm minimization. In *Proceedings of the Twenty-Fifth Conference on Uncertainty in Artificial Intelligence*, pages 339–348, 2009.
- [29] Ali Jalali, Sujay Sanghavi, Chao Ruan, and Pradeep Ravikumar. A dirty model for multi-task learning. *Advances in neural information processing systems*, 23, 2010.
- [30] Shengbo Guo, Onno Zoeter, and Cédric Archambeau. Sparse bayesian multi-task learning. *Advances in Neural Information Processing Systems*, 24, 2011.
- [31] Andrew Gelman, John B Carlin, Hal S Stern, David B Dunson, Aki Vehtari, and Donald B Rubin. *Bayesian data analysis*, volume 2. CRC press Boca Raton, FL, 2014.
- [32] Ya Xue, Xuejun Liao, Lawrence Carin, and Balaji Krishnapuram. Multi-task learning for classification with dirichlet process priors. *Journal of Machine Learning Research*, 8(1), 2007.
- [33] Yi Zhang and Jeff Schneider. Learning multiple tasks with a sparse matrix-normal penalty. *Advances in neural information processing systems*, 23, 2010.
- [34] Andre Goncalves, Priyadip Ray, Braden Soper, David Widemann, Mari Nygård, Jan F Nygård, and Ana Paula Sales. Bayesian multitask learning regression for heterogeneous patient cohorts. *Journal of Biomedical Informatics*, 100:100059, 2019.
- [35] Cécile Bazot, Nicolas Dobbigeon, Jean-Yves Tourneret, and Alfred O Hero. A bernoulli-gaussian model for gene factor analysis. In *2011 IEEE International Conference on Acoustics, Speech and Signal Processing (ICASSP)*, pages 5996–5999. IEEE, 2011.
- [36] David M Blei, Alp Kucukelbir, and Jon D McAuliffe. Variational inference: A review for statisticians. *Journal of the American statistical Association*, 112(518):859–877, 2017.
- [37] Cheng Zhang, Judith Bütepage, Hedvig Kjellström, and Stephan Mandt. Advances in variational inference. *IEEE transactions on pattern analysis and machine intelligence*, 41(8):2008–2026, 2018.
- [38] Car Reen Kok, Nisha J Mulakken, James B Thissen, Jose Manuel Marti, Ryan Lee, Jacob B Trainer, Andre R Goncalves, Hiranmayi Ranganathan, Aram Avila-Herrera, Crystal J Jaing, et al. Meta2db: Curated shotgun metagenomic feature sets and metadata for health state prediction. *bioRxiv*, pages 2024–10, 2024.
- [39] Shifu Chen, Yanqing Zhou, Yaru Chen, and Jia Gu. fastp: an ultra-fast all-in-one fastq preprocessor. *Bioinformatics*, 34(17):i884–i890, 2018.
- [40] Daehwan Kim, Li Song, Florian P Breitwieser, and Steven L Salzberg. Centrifuge: rapid and sensitive classification of metagenomic sequences. *Genome research*, 26(12):1721–1729, 2016.
- [41] Jose Manuel Marti, Car Reen Kok, James B Thissen, Nisha J Mulakken, Aram Avila-Herrera, Crystal J Jaing, Jonathan E Allen, and Nicholas A Be. Addressing the dynamic nature of reference data: a new nt database for robust metagenomic classification. *bioRxiv*, pages 2024–06, 2024.

- [42] NCBI Resource Coordinators. Database resources of the national center for biotechnology information. *Nucleic acids research*, 41(D1):D8–D20, 2012.
- [43] Jose Manuel Martí. Recentrifuge: Robust comparative analysis and contamination removal for metagenomics. *PLoS computational biology*, 15(4):e1006967, 2019.
- [44] John Aitchison. The statistical analysis of compositional data. *Journal of the Royal Statistical Society: Series B (Methodological)*, 44(2):139–160, 1982.
- [45] Robert Tibshirani. Regression shrinkage and selection via the lasso. *Journal of the Royal Statistical Society: Series B (Methodological)*, 58(1):267–288, 1996.
- [46] Onureena Banerjee, Laurent El Ghaoui, and Alexandre d’Aspremont. Model selection through sparse maximum likelihood estimation for multivariate gaussian or binary data. *The Journal of Machine Learning Research*, 9:485–516, 2008.
- [47] Baohong Wang, Mingfei Yao, Longxian Lv, Zongxin Ling, and Lanjuan Li. The human microbiota in health and disease. *Engineering*, 3(1):71–82, 2017.
- [48] Charles Sossun, Jérôme Idier, David Brie, and Junbo Duan. From bernoulli–gaussian deconvolution to sparse signal restoration. *IEEE Transactions on Signal Processing*, 59(10):4572–4584, 2011.
- [49] Christopher M Bishop and Nasser M Nasrabadi. *Pattern recognition and machine learning*, volume 4 of *Information Science and Statistics*. Springer, 2006.
- [50] Dankmar Böhning and Bruce G Lindsay. Monotonicity of quadratic-approximation algorithms. *Annals of the Institute of Statistical Mathematics*, 40(4):641–663, 1988.
- [51] David R Hunter and Kenneth Lange. A tutorial on mm algorithms. *The American Statistician*, 58(1):30–37, 2004.
- [52] Tommi S Jaakkola and Michael I Jordan. A variational approach to bayesian logistic regression models and their extensions. In *Sixth International Workshop on Artificial Intelligence and Statistics*, pages 283–294. PMLR, 1997.
- [53] Jan Drugowitsch. Variational bayesian inference for linear and logistic regression. *arXiv preprint arXiv:1310.5438*, 2013.
- [54] Jerome Friedman, Trevor Hastie, and Robert Tibshirani. Sparse inverse covariance estimation with the graphical lasso. *Biostatistics*, 9(3):432–441, 2008.
- [55] Rahul Mazumder and Trevor Hastie. The graphical lasso: New insights and alternatives. *Electronic journal of statistics*, 6:2125, 2012.
- [56] Ron Kohavi et al. A study of cross-validation and bootstrap for accuracy estimation and model selection. In *Ijcai*, volume 14, pages 1137–1145. Montreal, Canada, 1995.
- [57] Alexandru Niculescu-Mizil and Rich Caruana. Predicting good probabilities with supervised learning. In *Proceedings of the 22nd international conference on Machine learning*, pages 625–632, 2005.
- [58] Lawrence A David, Ana Weil, Edward T Ryan, Stephen B Calderwood, Jason B Harris, Fahima Chowdhury, Yasmin Begum, Firdausi Qadri, Regina C LaRocque, and Peter J Turnbaugh. Gut microbial succession follows acute secretory diarrhea in humans. *MBio*, 6(3):10–1128, 2015.
- [59] Silas Kieser, Shafiqul A Sarker, Olga Sakwinska, Francis Foata, Shamima Sultana, Zeenat Khan, Shoheb Islam, Nadine Porta, Séverine Combremont, Bertrand Betrisey, et al. Bangladeshi children with acute diarrhoea show faecal microbiomes with increased streptococcus abundance, irrespective of diarrhoea aetiology. *Environmental microbiology*, 20(6):2256–2269, 2018.
- [60] Daniel McDonald, Embriette Hyde, Justine W Debelius, James T Morton, Antonio Gonzalez, Gail Ackermann, Alexander A Aksenov, Bahar Behsaz, Caitriona Brennan, Yingfeng Chen, et al. American gut: an open platform for citizen science microbiome research. *Msystems*, 3(3):10–1128, 2018.
- [61] Roy M Robins-Browne and Elizabeth L Hartland. *Escherichia coli* as a cause of diarrhea. *Journal of gastroenterology and hepatology*, 17(4):467–475, 2002.
- [62] Pablo C Okhuysen and Herbert L DuPont. Enteroaggregative *escherichia coli* (eae): a cause of acute and persistent diarrhea of worldwide importance, 2010.
- [63] Courtney D Petro, Jeffrey K Duncan, Yuliya I Seldina, Anna Allué-Guardia, Mark Eppinger, Mark S Riddle, David R Tribble, Ryan C Johnson, Clifton L Dalgard, Gauthaman Sukumar, et al. Genetic and virulence profiles of enteroaggregative *escherichia coli* (eae) isolated from deployed military personnel (dmp) with travelers’ diarrhea. *Frontiers in Cellular and Infection Microbiology*, 10:200, 2020.
- [64] Linda Smith, Ekaterina Goldobina, Bianca Govi, and Andrey N Shkoporov. Bacteriophages of the order crassvirales: what do we currently know about this keystone component of the human gut virome? *Biomolecules*, 13(4):584, 2023.
- [65] Ann C Gregory, Olivier Zablocki, Ahmed A Zayed, Allison Howell, Benjamin Bolduc, and Matthew B Sullivan. The gut virome database reveals age-dependent patterns of virome diversity in the human gut. *Cell host & microbe*, 28(5):724–740, 2020.
- [66] Shahrzad Ezzatpour, Alicia del Carmen Mondragon Portocarrero, Alejandra Cardelle-Cobas, Alexandre Lamas, Aroa López-Santamarina, José Manuel Miranda, and Hector C Aguilar. The human gut virome and its relationship with nontransmissible chronic diseases. *Nutrients*, 15(4):977, 2023.
- [67] Qiyun Zhu, Christopher L Dupont, Marcus B Jones, Kevin M Pham, Zhi-Dong Jiang, Herbert L DuPont, and Sarah K Highlander. Visualization-assisted binning of metagenome assemblies reveals potential new pathogenic profiles in idiopathic travelers’ diarrhea. *Microbiome*, 6:1–20, 2018.
- [68] Andrey N Shkoporov, Adam G Clooney, Thomas DS Sutton, Feargal J Ryan, Karen M Daly, James A Nolan, Siobhan A McDonnell, Ekaterina V Khokhlova, Lorraine A Draper, Amanda Forde, et al. The human gut virome is highly diverse, stable, and individual specific. *Cell host & microbe*, 26(4):527–541, 2019.
- [69] Andrey N Shkoporov, Orla O’Regan, Linda Smith, Ekaterina V Khokhlova, Lorraine A Draper, R Paul Ross, and Colin Hill. Dynamic nature of viral and bacterial communities in human faeces. *Iscience*, 27(2), 2024.

Haonan Zhu received the Ph.D. degree in electrical and computer engineering from the University of Michigan in 2023. He is currently a Postdoctoral Researcher with the Lawrence Livermore National Laboratory.

Andre R Goncalves received the Ph.D. degree in electrical and computer engineering from the University of Campinas in Brazil in 2016. He is currently a Machine Learning Research Scientist with the Lawrence Livermore National Laboratory.

Hiranmayi Ranganathan received her Ph.D. degree in Deep Learning from Arizona State University in 2018. She is currently Group Leader of the Computer Vision Group with Lawrence Livermore National Laboratory.

Camilo Valdes received his Ph.D. degree in Computer Science from the School of Computing and Information Sciences at Florida International University. He is currently a Postdoctoral Researcher in the Physical and Life Sciences Directorate at Lawrence Livermore National Laboratory.

Boya Zhang received her Ph.D. in statistics from the Virginia Tech in 2020. She is now a Staff Scientist at Lawrence Livermore National Laboratory.

Jose Manuel Martí received a Ph.D. in Computational Biology and an M.Sc. in Astrophysics from the University of Valencia (est. 1498). He is an engineer at Lawrence Livermore National Laboratory and an affiliate at Berkeley Lab.

Car Reen Kok received a Ph.D. degree in Complex Biosystems from the University of Nebraska-Lincoln. She is a Postdoctoral Researcher in the Microbiology/Immunology group at Lawrence Livermore National Laboratory.

Monica Borucki received her Ph.D. degree in Microbiology from Colorado State University. She is currently a Biomedical Scientist at Lawrence Livermore National Laboratory.

Nisha Mulakken received a M.A. degree in biostatistics from UC Berkeley and B.S. degree in Genetics from UC Davis. She is currently a Group Leader and Bioinformatics Software Developer at Lawrence Livermore National Laboratory.

James Thissen received a Masters degree in bioinformatics from the Johns Hopkins University in 2017. He is currently a researcher with Lawrence Livermore National Laboratory.

Crystal Jaing received her Ph.D. in Molecular Biology and Biochemistry from Indiana University School of Medicine. She is currently a research scientist at Lawrence Livermore National Lab.

Alfred Hero (Life Fellow of the IEEE) received the PhD in Electrical Engineering and Computer Science from Princeton University. He is the John H. Holland Distinguished University Professor of Electrical Engineering and Computer Science and the R. Jamison and Betty Williams Professor of Engineering at the University of Michigan, Ann Arbor.

Nicholas A. Be received a Ph.D. degree in Cellular and Molecular Medicine from the Johns Hopkins University School of Medicine. He is the Group Leader for Microbiology/Immunology at Lawrence Livermore National Laboratory.

Supplementary: Hierarchical Bayesian Multitask Model for Microbiome Analysis

Haonan Zhu^{1,2,*}, Andre R. Goncalves^{1,*}, Camilo Valdes¹, Hiranmayi Ranganathan¹, Boya Zhang¹, Jose Manuel Martí¹, Car Reen Kok¹, Monica K. Borucki¹, Nisha J. Mulakken¹, James B. Thissen¹, Crystal Jaing¹, Alfred Hero², and Nicholas A. Be^{1,*}

¹Lawrence Livermore National Laboratory

²Electrical and Computer Engineering, University of Michigan

*Corresponding Authors: zhu18@llnl.gov, andre@llnl.gov, be1@llnl.gov

I. DATASET REFERENCES

Table I include references to all the studies used in this work along with their metadata. Some studies were obtained from the curatedMetagenomicData package [1].

TABLE I: Summary of microbiome studies by disease categories. Notably [2] contains two diseases (age-related macular degeneration, cardiovascular disease) and [3] contains six diseases (diabetes, neurological disease, irritable bowel syndrome, inflammatory bowel disease, gastrointestinal infection and diarrhea, therefore they are split into multiple studies based on the disease categories for our analysis.

Disease Category	Ref.	Host Body Site	Geographic Location	Control and Disease Splits (C/D)
Diabetes	[4]	Fecal	Europe	43/102
	[5]	Fecal	United States	17/19
	[6]	Fecal	Luxembourg	26/27
	[3]	Fecal	United States	359/19
Cirrhosis	[7]	Fecal	China	113/110
	[8]	Fecal	United States	77/9
Cancer	[9]	Fecal	Austria	61/93
	[10]	Fecal	China	53/75
	[11]	Fecal	North America	21/36
	[12]	Fecal	Japan	250/365
	[13]	Fecal, Oral	Not Available	470/90
Neurological Disease	[14]	Oral	United States	16/16
	[15]	Fecal	United States	50/50
	[16]	Fecal	China	40/40
	[17]	Fecal	China	81/90
	[18]	Fecal, Oral	South Korea	74/81
	[19]	Fecal	Germany	100/75
	[20]	Fecal	United States	233/491

Continued on next page

TABLE I – continued from previous page

Disease Category	Ref.	Host Body Site	Geographic Location	Control and Disease Splits (C/D)
	[3]	Fecal	United States	359/253
Diarrhea	[21]	Fecal, Rectal Swab	Bangladesh	7/23
	[22]	Fecal	Bangladesh	9/18
	[3]	Fecal	United States	359/60
Dermatologic Disease	[23]	Skin	Asia	40/38
	[24]	Skin	United States	53/238
	[25]	Skin	Singapore	50/69
	[26]	Fecal	United States	15/33
Gastrointestinal Infection	[27]	Fecal	Canada	182/27
	[28]	Fecal	Indonesia, Liberia	5/19
	[29]	Fecal	Cameroon	86/89
	[3]	Fecal	United States	359/5
Inflammatory Bowel Disease	[30]	Fecal	United States	71/175
	[31]	Fecal	Not Available	56/162
	[32]	Fecal	Not Available	354/888
	[33]	Fecal	United States	27/8
	[3]	Fecal	United States	359/9
Cardiovascular Disease	[34]	Fecal	China	171/214
	[35]	Fecal	China	41/155
	[36]	Fecal	China	56/60
	[37]	Fecal	United States	27/127
	[38]	Fecal	China	10/10
	[2]	Fecal	Switzerland	30/29
Oral Disease	[39]	Oral	Australia	37/48
	[40]	Oral	Italy	51/23
	[41]	Oral	Hungary	8/19
Autoimmune Disease	[42]	Fecal	China	45/20
	[43]	Fecal	China	62/100

Continued on next page

TABLE I – continued from previous page

Disease Category	Ref.	Host Body Site	Geographic Location	Control and Disease Splits (C/D)
Immune Disease	[44]	Fecal	Spain	27/129
Pulmonary Disease	[45]	Fecal	China	31/46
	[46]	Cough Swabs	Germany	48/49
	[47]	Fecal	China	15/55
	[48]	Nasal	Sweden	20/37
	[49]	Fecal	China	63/47
	[50]	Lung (Bronchioalveolar Lavage Fluid)	China	16/45
	[51]	Fecal	China	69/138
[52]	Fecal	China	21/20	
Metabolic Disease	[53]	Fecal	Mexico	10/10
Hormonal Disorder	[54]	Fecal	China	43/50
Genitourinary Disease	[55]	Endocervical, Vaginal, Rectal	Fiji	11/14
Seafaring Syndrome	[56]	Fecal	Not Available	99/55
Irritable Bowel Syndrome	[3]	Fecal	United States	359/52
Age-Related Macular Degeneration	[2]	Fecal	Switzerland	33/57

II. CAVI UPDATE DERIVATION

This section includes the derivations of CAVI updates for Algorithm I.

Recall Equation 18 of [57] states that if we are to approximate a general posterior distribution $p(\xi \mid \text{data})$ with a mean-field approximation $q(\xi) := \prod_j q_j(\xi_j)$, the CAVI update for j -th latent variable ξ_j (i.e., the optimal solution $q_j^*(\xi_j)$) is proportional to the exponentiated conditional expected log of the joint:

$$q_j^* \propto \exp\left(\mathbb{E}_{\xi_{-j} \sim q_{-j}} [\log(p(\xi_j, \xi_{-j} \mid \text{data}))]\right). \quad (1)$$

where ξ_{-j} corresponds to all but the j -th latent variable.

a) *Update for α, β* : Based on Eqn. 1, the exponentiated conditional expectation of all the parameters except θ up to a constant scaling factor:

$$\begin{aligned} q^*(\theta) &\propto \exp((\alpha_0 - 1) \log \theta + (\beta_0 - 1) \log(1 - \theta)) \\ &\quad \exp\left(\left(\sum_j \phi_j\right) \log \theta + \left(d - \sum_j \phi_j\right) \log(1 - \theta)\right) \\ &= \exp\left(\left(\alpha_0 - 1 + \sum_j \phi_j\right) \log \theta\right) \\ &\quad \exp\left(\left(\beta_0 + d - \sum_j \phi_j - 1\right) \log(1 - \theta)\right). \end{aligned}$$

This implies $q^*(\theta)$ follows a beta distribution with parameters:

$$\begin{aligned} \alpha &= \alpha_0 + \sum_j \phi_j, \\ \beta &= \beta_0 + d - \sum_j \phi_j. \end{aligned}$$

b) *Update for v and \mathbf{V}* : Based on Eqn. 1, the exponentiated conditional expectation of all the parameters except Σ_0^{-1} up to a constant scaling factor:

$$\begin{aligned} q^*(\Sigma_0^{-1}) &\propto \exp\left(-\frac{1}{2} \text{tr}(\mathbf{V}_0^{-1} \Sigma_0^{-1})\right) \\ &\quad \exp\left(-\frac{v_0 + d - T - 1}{2} \log \det(\Sigma_0^{-1})\right) \\ &\quad \exp\left(-\frac{1}{2} \text{tr}\left(\Sigma_0^{-1} \left(\sum_j \mathbf{m}_{(j)} \mathbf{m}_{(j)}^\top + \Sigma_j\right)\right)\right). \end{aligned}$$

This implies $q^*(\Sigma_0^{-1})$ follow a Wishart distribution with parameters:

$$\begin{aligned} v &= v_0 + d, \\ \mathbf{V} &= \left(\mathbf{V}_0^{-1} + \sum_j \mathbf{m}_{(j)} \mathbf{m}_{(j)}^\top + \Sigma_j\right)^{-1}. \end{aligned}$$

c) *Update for Σ_j* : all the terms involve Σ_j in ELBO approximation (Eqn. 3, section III.A):

$$-\frac{1}{2} \text{tr}(v \mathbf{V} \Sigma_j) - \frac{1}{8} \sum_t (\Sigma_j)_{t,t} \phi_j \sum_i (x_t^{ij})^2 + \frac{1}{2} \log \det(\Sigma_j).$$

Rewrite the second term:

$$-\frac{1}{8} \text{tr}\left(\Sigma_j \text{diag}\left(\left[\sum_i \phi_j (x_1^{ij})^2, \dots, \sum_i \phi_j (x_T^{ij})^2\right]^\top\right)\right).$$

Denote the diagonal matrix as $\tilde{\mathbf{X}}_j$. For every j , we have a constrained optimization problem:

$$\max_{\Sigma \in \mathbb{S}_{++}^T} \log \det (\Sigma) - \text{tr} \left(\Sigma \left(v \mathbf{V} + \frac{1}{4} \tilde{\mathbf{X}}_j \right) \right).$$

which admits a closed form solution:

$$\Sigma_j^* = \left(v \mathbf{V} + \frac{1}{4} \tilde{\mathbf{X}}_j \right)^{-1}. \quad (2)$$

for $j = 1, \dots, d$.

d) Update for $\mathbf{m}_{(j)}$: all the terms involved $\mathbf{m}_{(j)}$ in ELBO approximation (Eqn. 3, section III.A):

$$\begin{aligned} & -\frac{v}{2} \langle \mathbf{m}_{(j)}, \mathbf{V} \mathbf{m}_{(j)} \rangle - \frac{1}{8} \langle \mathbf{m}_{(j)}, \tilde{\mathbf{X}}_j \mathbf{m}_{(j)} \rangle \\ & + \left\langle \mathbf{m}_{(j)}, \left[\dots, \phi_j \sum_i (y_t^i - \tilde{y}_t^i) x_t^{ij}, \dots \right]^\top \right\rangle \\ & + \frac{1}{4} \left\langle \mathbf{m}_{(j)}, \left[\dots, \phi_j \sum_i \langle \mathbf{w}'_t \circ \mathbf{z}', \mathbf{x}_t^i \rangle x_t^{ij}, \dots \right]^\top \right\rangle \\ & - \frac{1}{4} \left\langle \mathbf{m}_{(j)}, \left[\dots, \phi_j \sum_i x_t^{ij} \sum_{l \neq j} \phi_l x_t^{il} m_{tl}, \dots \right]^\top \right\rangle. \end{aligned}$$

This problem is quadratic with a negative definite Hessian matrix, hence by stationary condition (i.e., zero gradient) we have closed form updates:

$$\begin{aligned} & \Sigma_j^* \left(\left[\dots, \phi_j \sum_i (y_t^i - \tilde{y}_t^i) x_t^{ij}, \dots \right]^\top \right. \\ & \quad + \frac{1}{4} \left[\dots, \phi_j \sum_i \langle \mathbf{w}'_t \circ \mathbf{z}', \mathbf{x}_t^i \rangle x_t^{ij}, \dots \right]^\top \\ & \quad \left. - \frac{1}{4} \left[\dots, \phi_j \sum_i x_t^{ij} \sum_{l \neq j} \phi_l x_t^{il} m_{tl}, \dots \right]^\top \right). \end{aligned} \quad (3)$$

For all $j = 1 \dots, d$. When the reference point of quadratic lower bound $\mathbf{w}' \circ \mathbf{z}'$ is set to be the mean parameters from the previous iteration, we can simplify Eqn. 4:

$$\begin{aligned} & \Sigma_j^* \left(\left[\phi_j \sum_i (y_1^i - \tilde{y}_1^i) x_1^{ij}, \dots, \phi_j \sum_i (y_T^i - \tilde{y}_T^i) x_T^{ij} \right]^\top \right. \\ & \quad \left. + \frac{1}{4} \left[\phi_j^2 \sum_i (x_1^{ij})^2 m_{1j}^{(k)}, \dots, \phi_j^2 \sum_i (x_T^{ij})^2 m_{Tj}^{(k)} \right]^\top \right). \end{aligned} \quad (4)$$

e) Update for ϕ_j : All the terms involve ϕ_j in ELBO approximation (Eqn. 3, section III.A):

$$\begin{aligned} f(\phi_j) & := \phi_j (\psi(\alpha) - \psi(\beta)) + \phi_j \sum_t \sum_i (y_t^i - \tilde{y}_t^i) m_{tj} x_t^{ij} \\ & \quad + \frac{\phi_j}{4} \sum_t \sum_i (m_{tj} x_t^{ij}) \langle \mathbf{w}'_t \circ \mathbf{z}', \mathbf{x}_t^i \rangle \\ & \quad - \frac{\phi_j}{4} \sum_t \sum_i m_{tj} x_t^{ij} \sum_{l \neq j} m_{tl} \phi_l x_t^{il} \\ & \quad - \frac{\phi_j}{8} \sum_t ((\Sigma_j)_{tt} + m_{tj}^2) \sum_i (x_t^{ij})^2 \\ & \quad - \phi_j \log(\phi_j) - (1 - \phi_j) \log(1 - \phi_j). \end{aligned}$$

Observe $f(\phi_j)$ is a smooth strictly concave function, so we can solve for ϕ_j^* by stationary condition (i.e., 0 derivatives), which admit a closed form update:

$$\phi_j^* = \sigma(a). \quad (5)$$

where $\sigma(t) := \frac{1}{\exp(-t)+1}$ denote the sigmoid function, and:

$$\begin{aligned} a = & \psi(\alpha) - \psi(\beta) + \sum_t \sum_i \left(y_t^i - \tilde{y}_t^i \right) m_{tj} x_t^{ij} \\ & + \frac{1}{4} \sum_t \sum_i \left(m_{tj} x_t^{ij} \right) \langle \mathbf{w}'_t \circ \mathbf{z}', \mathbf{x}_t^i \rangle \\ & - \frac{1}{4} \sum_t \sum_i m_{tj} x_t^{ij} \sum_{l \neq j} m_{tl} \phi_l x_t^{il} \\ & - \frac{1}{8} \sum_t \left((\Sigma_j)_{tt} + m_{tj}^2 \right) \sum_i \left(x_t^{ij} \right)^2. \end{aligned}$$

When reference point of quadratic lower bound $\mathbf{w}' \circ \mathbf{z}'$ is set to be the mean parameters from the previous iterations, Eqn. 5 is simplified:

$$\phi_j^{k+1} = \sigma(a). \quad (6)$$

where

$$\begin{aligned} a = & \psi(\alpha) - \psi(\beta) + \sum_t \sum_i \left(y_t^i - \tilde{y}_t^i \right) m_{tj} x_t^{ij} \\ & + \frac{1}{8} \sum_t \left(m_{tj}^2 \left(2\phi_j^{(k)} - 1 \right) - (\Sigma_j)_{tt} \right) \sum_i \left(x_t^{ij} \right)^2. \end{aligned}$$

III. ADDITIONAL EXPERIMENTAL RESULTS

This section includes additional experimental results. We exam the methods using more evaluation metrics including: accuracy, balanced accuracy, averaged precision, F1 score, F2 score, and Matthews correlation coefficient (MCC). Table II summarizes the definitions of these metrics.

A. Synthetic Datasets

This subsection include the detailed experimental results on the synthetic datasets summarized in Table III

B. Microbiome Data

This subsection include the additional experimental results on the microbiome data: table IV includes the evaluations of the prediction performance, Fig. 1 and Fig. 2 include the predicted probabilities on training and test data for the other taxonomic ranks respectively, Fig. 3 includes the additional calibration curves.

Metric	Definition
TP	$\sum_{i=1}^N \mathbf{1}(y_i = 1 \wedge \hat{y}_i = 1)$
TN	$\sum_{i=1}^N \mathbf{1}(y_i = 0 \wedge \hat{y}_i = 0)$
FP	$\sum_{i=1}^N \mathbf{1}(y_i = 0 \wedge \hat{y}_i = 1)$
FN	$\sum_{i=1}^N \mathbf{1}(y_i = 1 \wedge \hat{y}_i = 0)$
Precision	$\frac{TP}{TP+FP}$
Recall	$\frac{TP}{TP+FN}$
Accuracy	$\frac{TP+TN}{N}$
Balanced Accuracy	$\frac{1}{2} \left(\frac{TP}{TP+FN} + \frac{TN}{TN+FP} \right)$
F1 Score	$\frac{2 \cdot \text{Precision} \cdot \text{Recall}}{\text{Precision} + \text{Recall}}$
F2 Score	$\frac{5 \cdot \text{Precision} \cdot \text{Recall}}{4 \cdot \text{Precision} + \text{Recall}}$
MCC	$\frac{(TP \cdot TN) - (FP \cdot FN)}{\sqrt{(TP+FP)(TP+FN)(TN+FP)(TN+FN)}}$

TABLE II: Definitions of classification metrics and the intermediate variables given ground truth labels \mathbf{y} and predicted labels $\hat{\mathbf{y}}$. \wedge denotes the "and" operation, and $\mathbf{1}(\cdot)$ is the indicator function, which is 1 if the condition inside is true and 0 otherwise.

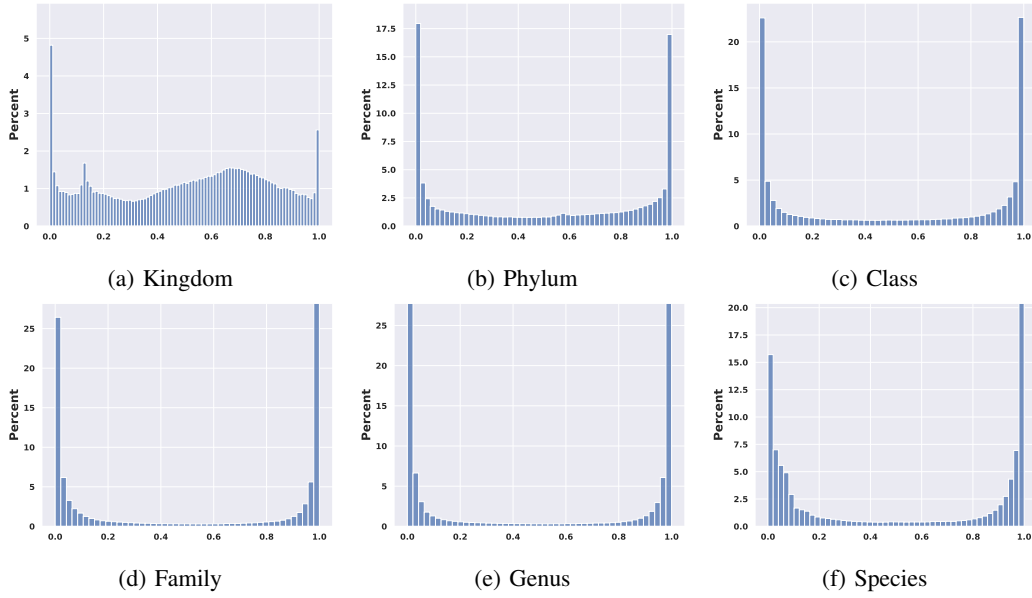


Fig. 1: Histogram of predicted probabilities on training data for different taxonomic ranks.

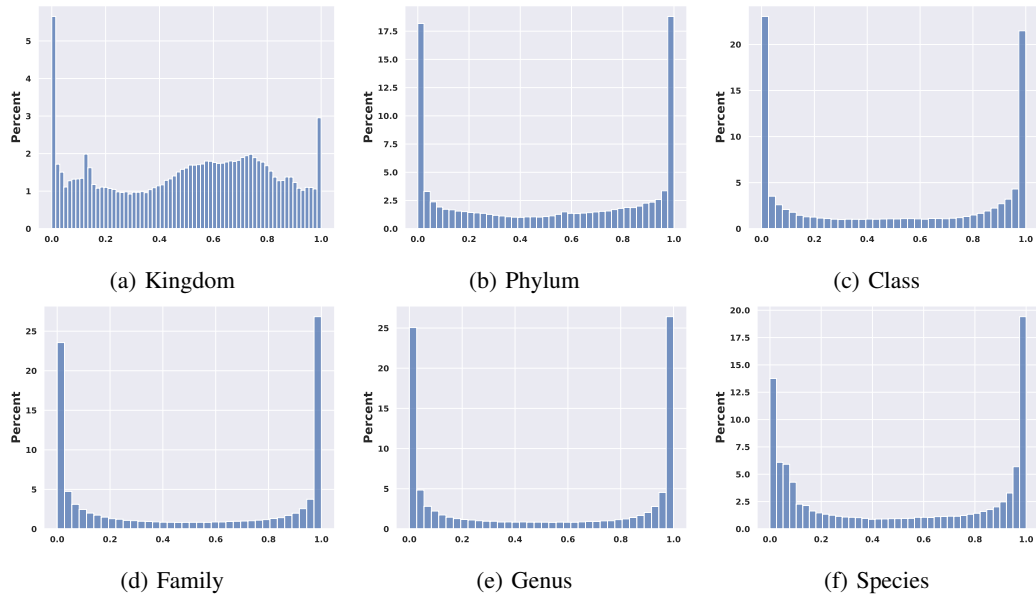


Fig. 2: Histogram of predicted probabilities on test data for different taxonomic ranks.

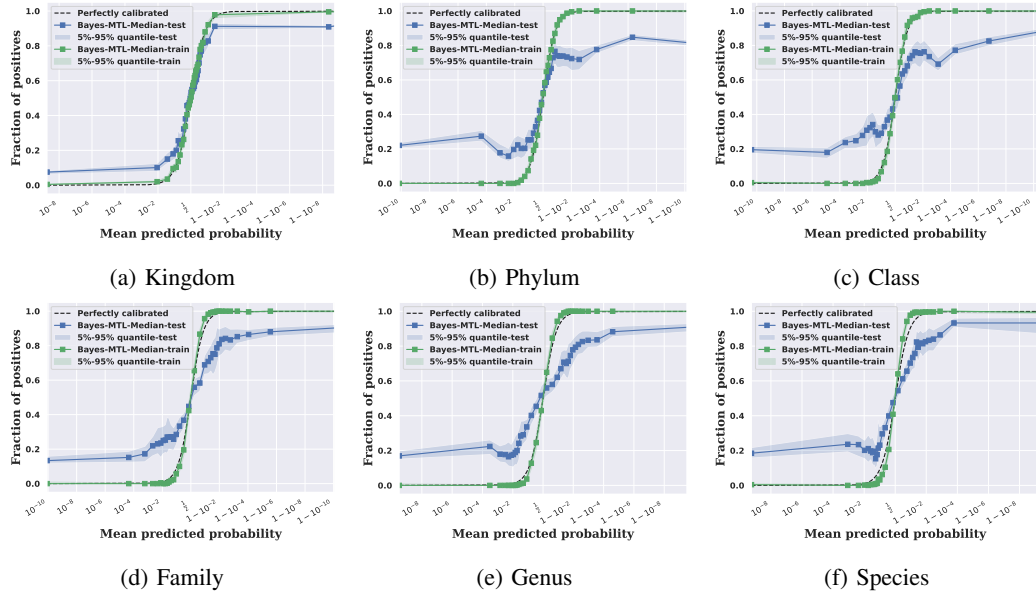


Fig. 3: Calibration curves for different taxonomic ranks.

Dataset	Metrics	BayesMTL	MTFL	MSSL	STL-LC	Pooled-LC
dataset1 (dense, balanced)	Accuracy	0.322 (0.06)	0.793 (0.05)	0.793 (0.05)	0.688 (0.05)	0.71 (0.04)
	Balanced Accuracy	0.565 (0.03)	0.5 (0)	0.5 (0)	0.525 (0.05)	0.52 (0.03)
	Average Precision	0.819 (0.05)	0.793 (0.05)	0.793 (0.05)	0.803 (0.04)	0.800 (0.05)
	F1 Score	0.261 (0.06)	0.884 (0.03)	0.884 (0.03)	0.801 (0.04)	0.821 (0.03)
	F2 Score	0.183 (0.05)	0.950 (0.01)	0.950 (0.01)	0.800 (0.05)	0.834 (0.03)
	MCC	0.156 (0.06)	0 (0)	0 (0)	0.0565 (0.09)	0.0427 (0.07)
dataset2 (sparse, balanced)	Accuracy	0.882 (0.04)	0.225 (0.03)	0.225 (0.03)	0.438 (0.08)	0.364 (0.02)
	Balanced Accuracy	0.768 (0.05)	0.5 (0)	0.5 (0)	0.616 (0.05)	0.548 (0.04)
	Average Precision	0.597 (0.10)	0.225 (0.03)	0.225 (0.03)	0.279 (0.06)	0.244 (0.02)
	F1 Score	0.681 (0.09)	0.367 (0.03)	0.367 (0.03)	0.431 (0.07)	0.383 (0.03)
	F2 Score	0.602 (0.09)	0.590 (0.03)	0.590 (0.03)	0.634 (0.06)	0.579 (0.04)
	MCC	0.638 (0.10)	0 (0)	0 (0)	0.227 (0.09)	0.104 (0.07)
dataset3 (ultra sparse, balanced)	Accuracy	0.988 (0.02)	0.0350 (0.01)	0.0350 (0.01)	0.437 (0.08)	0.199 (0.04)
	Balanced Accuracy	0.947 (0.06)	0.5 (0)	0.5 (0)	0.708 (0.04)	0.526 (0.09)
	Average Precision	0.801 (0.20)	0.035 (0.01)	0.035 (0.01)	0.0584 (0.01)	0.0372 (0.01)
	F1 Score	0.876 (0.13)	0.0674 (0.02)	0.0674 (0.02)	0.110 (0.02)	0.070 (0.02)
	F2 Score	0.886 (0.12)	0.152 (0.04)	0.152 (0.04)	0.235 (0.05)	0.154 (0.04)
	MCC	0.879 (0.13)	0 (0)	0 (0)	0.154 (0.02)	0.0199 (0.08)
dataset4 (dense, unbalanced)	Accuracy	0.441 (0.12)	0.795 (0.04)	0.795 (0.04)	0.689 (0.09)	0.693 (0.04)
	Balanced Accuracy	0.584 (0.06)	0.5 (0)	0.5 (0)	0.554 (0.07)	0.517 (0.04)
	Average Precision	0.827 (0.04)	0.795 (0.04)	0.795 (0.04)	0.814 (0.04)	0.801 (0.04)
	F1 Score	0.483 (0.16)	0.885 (0.02)	0.885 (0.02)	0.794 (0.08)	0.808 (0.03)
	F2 Score	0.393 (0.15)	0.951 (0.01)	0.951 (0.01)	0.788 (0.12)	0.813 (0.04)
	MCC	0.147 (0.09)	0 (0)	0 (0)	0.118 (0.12)	0.039 (0.08)
dataset5 (sparse, unbalanced)	Accuracy	0.796 (0.07)	0.219 (0.04)	0.219 (0.04)	0.451 (0.07)	0.334 (0.03)
	Balanced Accuracy	0.783 (0.06)	0.5 (0)	0.5 (0)	0.626 (0.036)	0.541 (0.04)
	Average Precision	0.472 (0.13)	0.219 (0.04)	0.219 (0.04)	0.275 (0.05)	0.234 (0.03)
	F1 Score	0.625 (0.1)	0.358 (0.05)	0.358 (0.05)	0.427 (0.06)	0.370 (0.04)
	F2 Score	0.694 (0.05)	0.579 (0.06)	0.579 (0.06)	0.630 (0.05)	0.569 (0.04)
	MCC	0.516 (0.13)	0 (0)	0 (0)	0.240 (0.05)	0.086 (0.08)
dataset6 (ultra sparse, unbalanced)	Accuracy	0.917 (0.10)	0.059 (0.0239)	0.059 (0.0239)	0.478 (0.07)	0.21 (0.04)
	Balanced Accuracy	0.905 (0.08)	0.5 (0)	0.5 (0)	0.715 (0.05)	0.553 (0.03)
	Average Precision	0.598 (0.02)	0.059 (0.02)	0.059 (0.02)	0.097 (0.03)	0.0646 (0.02)
	F1 Score	0.699 (0.27)	0.11 (0.04)	0.11 (0.04)	0.176 (0.05)	0.120 (0.04)
	F2 Score	0.763 (0.20)	0.233 (0.08)	0.233 (0.08)	0.343 (0.08)	0.246 (0.07)
	MCC	0.704 (0.26)	0 (0)	0 (0)	0.198 (0.03)	0.063 (0.03)

TABLE III: Summary of the support recovery results for the simulated data. The bold number means the corresponding method is the best performing algorithm for the given metrics and dataset, and the values in parentheses represent standard deviations computed over 10 different runs. The proposed Bayesian approach outperforms the benchmark methods in all evaluation metrics when there is a shared sparsity structure across regression coefficients of different tasks. Both MSSL and MTFL prioritize the prediction performance in the cross-validation step which results in complete dense solutions (i.e all regression coefficients are non-zero), hence they have identical results.

Taxon Ranks	Metrics	BayesMTL	MTFL	MSSL	Pooled-LC	STL-LC
Kingdom	Accuracy	0.681 (0.00956)	0.685 (0.0116)	0.685 (0.0121)	0.532 (0.00974)	0.618 (0.00725)
	Average Precision	0.572 (0.00897)	0.578 (0.00981)	0.582 (0.00999)	0.542 (0.00297)	0.57 (0.00872)
	Balanced Accuracy	0.578 (0.0131)	0.581 (0.0124)	0.589 (0.0137)	0.531 (0.00856)	0.584 (0.0105)
	F1 Score	0.588 (0.0163)	0.587 (0.0147)	0.59 (0.0121)	0.474 (0.0106)	0.523 (0.0284)
	F2 Score	0.602 (0.0182)	0.598 (0.0126)	0.598 (0.0104)	0.489 (0.0116)	0.547 (0.0365)
	mcc	0.171 (0.0281)	0.178 (0.0309)	0.19 (0.0345)	0.0622 (0.0169)	0.157 (0.0217)
	Sparsity Ratio	0.288 (0.0102)	0.541 (0.0298)	0.467 (0.0267)	0.883 (0.0408)	0.263 (0.0203)
Phylum	Accuracy	0.689 (0.0178)	0.715 (0.0159)	0.701 (0.0174)	0.552 (0.00715)	0.655 (0.01)
	Average Precision	0.598 (0.00862)	0.615 (0.00804)	0.621 (0.00927)	0.538 (0.00385)	0.593 (0.00802)
	Balanced Accuracy	0.618 (0.0146)	0.64 (0.0147)	0.651 (0.0151)	0.527 (0.0085)	0.612 (0.00993)
	F1 Score	0.614 (0.0153)	0.63 (0.018)	0.627 (0.0158)	0.521 (0.00613)	0.579 (0.0387)
	F2 Score	0.619 (0.0203)	0.63 (0.0222)	0.619 (0.0193)	0.536 (0.00786)	0.601 (0.0431)
	mcc	0.243 (0.0309)	0.294 (0.033)	0.302 (0.033)	0.0458 (0.0139)	0.222 (0.0223)
	Sparsity Ratio	0.182 (0.0169)	0.301 (0.00222)	0.311 (0.00286)	0.781 (0.0247)	0.0856 (0.012)
Class	Accuracy	0.688 (0.00922)	0.726 (0.0099)	0.695 (0.0156)	0.58 (0.0163)	0.668 (0.013)
	Average Precision	0.599 (0.0107)	0.625 (0.00884)	0.623 (0.0116)	0.548 (0.0061)	0.605 (0.00575)
	Balanced Accuracy	0.619 (0.013)	0.659 (0.0114)	0.656 (0.0167)	0.544 (0.0121)	0.629 (0.00728)
	F1 Score	0.619 (0.0143)	0.652 (0.0134)	0.632 (0.016)	0.54 (0.0155)	0.584 (0.0269)
	F2 Score	0.624 (0.0167)	0.657 (0.0155)	0.625 (0.0188)	0.552 (0.0159)	0.603 (0.037)
	mcc	0.245 (0.0261)	0.326 (0.0237)	0.307 (0.0324)	0.0803 (0.031)	0.26 (0.0151)
	Sparsity Ratio	0.116 (0.0121)	0.24 (0.00565)	0.295 (0.0531)	0.692 (0.019)	0.0697 (0.00536)
Order	Accuracy	0.698 (0.01)	0.703 (0.0116)	0.68 (0.012)	0.6 (0.00926)	0.68 (0.0142)
	Average Precision	0.609 (0.00955)	0.618 (0.00827)	0.622 (0.00906)	0.558 (0.0044)	0.617 (0.00803)
	Balanced Accuracy	0.634 (0.0126)	0.655 (0.0123)	0.659 (0.0131)	0.557 (0.00793)	0.645 (0.0119)
	F1 Score	0.629 (0.00964)	0.649 (0.018)	0.623 (0.0202)	0.553 (0.0147)	0.574 (0.0121)
	F2 Score	0.633 (0.0112)	0.659 (0.0238)	0.618 (0.0269)	0.566 (0.0169)	0.589 (0.0171)
	mcc	0.271 (0.0234)	0.309 (0.0279)	0.306 (0.0237)	0.112 (0.0148)	0.29 (0.023)
	Sparsity Ratio	0.109 (0.0115)	0.199 (0.00967)	0.222 (0.00103)	0.536 (0.00935)	0.046 (0.00772)
Family	Accuracy	0.704 (0.0218)	0.687 (0.0148)	0.665 (0.014)	0.608 (0.0162)	0.706 (0.00802)
	Average Precision	0.613 (0.0168)	0.625 (0.0144)	0.621 (0.0145)	0.567 (0.0104)	0.632 (0.00636)
	Balanced Accuracy	0.643 (0.0256)	0.658 (0.0149)	0.656 (0.0139)	0.57 (0.0179)	0.663 (0.00637)
	F1 Score	0.627 (0.0239)	0.62 (0.0171)	0.616 (0.0123)	0.565 (0.0172)	0.632 (0.0184)
	F2 Score	0.631 (0.0235)	0.609 (0.0223)	0.612 (0.0126)	0.574 (0.0164)	0.648 (0.0183)
	mcc	0.285 (0.0516)	0.307 (0.0286)	0.298 (0.0279)	0.134 (0.0366)	0.326 (0.00791)
	Sparsity Ratio	0.0429 (0.0151)	0.409 (x0.293)	0.172 (0.00179)	0.414 (0.00336)	0.0407 (0.00736)
x Genus	Accuracy	0.707 (0.00852)	0.65 (0.0291)	0.66 (0.0156)	0.619 (0.00865)	0.728 (0.0158)
	Average Precision	0.616 (0.00589) x	0.609 (0.0168)	0.62 (0.0123)	0.575 (0.00737)	0.647 (0.00831)
	Balanced Accuracy	0.641 (0.0109)	0.642 (0.0238)	0.657 (0.0135)	0.593 (0.0123)	0.683 (0.00959)
	F1 Score	0.634 (0.00774)	0.562 (0.109)	0.612 (0.0143)	0.579 (0.0167)	0.638 (0.0267)
	F2 Score	0.638 (0.00785)	0.562 (0.11)	0.61 (0.015)	0.589 (0.0219)	0.649 (0.0305)
	mcc	0.288 (0.0204)	0.272 (0.0468)	0.3 (0.0265)	0.175 (0.0246)	0.366 (0.02)
	Sparsity Ratio	0.0181 (0.00677)	0.403 (0.281)	0.152 (0.00116)	0.326 (0.00331)	0.0351 (0.00621)
Species	Accuracy	0.711 (0.0143)	0.57 (0.0205)	0.672 (0.0106)	0.648 (0.0113)	0.744 (0.0145)
	Average Precision	0.621 (0.015)	0.57 (0.00941)	0.628 (0.00825)	0.593 (0.00687)	0.66 (0.0119)
	Balanced Accuracy	0.65 (0.0168)	0.584 (0.0158)	0.671 (0.0117)	0.626 (0.0103)	0.7 (0.0132)
	F1 Score	0.635 (0.0168)	0.301 (0.0674)	0.622 (0.0108)	0.611 (0.00954)	0.651 (0.0222)
	F2 Score	0.634 (0.0146)	0.297 (0.0656)	0.618 (0.0136)	0.625 (0.0128)	0.661 (0.0244)
	mcc	0.305 (0.0333)	0.16 (0.0288)	0.325 (0.023)	0.234 (0.0202)	0.401 (0.0279)
	Sparsity Ratio	0.0289 (0.0053)	0.149 (0.0275)	0.149 (0.000836)	0.279 (0.00367)	0.0319 (0.00481)

TABLE IV: Summary of the prediction performance. The bold number means the corresponding method is the best performing algorithm for the given metrics and taxonomic rank, and the values in parentheses represent standard deviations computed over 5 different runs. Due to the heterogeneous nature of the data, we do not see an improvement of the proposed approach over single-task model. However, the proposed approach is the only multitask method that provides a sparse solution i.e identify common bacteria across studies of the same disease categories that are informative for the predictions.

REFERENCES

- [1] Edoardo Pasolli, Lucas Schiffer, Paolo Manghi, Audrey Renson, Valerie Obenchain, Duy Tin Truong, Francesco Beghini, Faizan Malik, Marcel Ramos, Jennifer B Dowd, et al. Accessible, curated metagenomic data through experimenthub. *Nature methods*, 14(11):1023–1024, 2017.
- [2] Denise C Zysset-Burri, Irene Keller, Lieselotte E Berger, Carlo R Largiadèr, Matthias Wittwer, Sebastian Wolf, and Martin S Zinkernagel. Associations of the intestinal microbiome with the complement system in neovascular age-related macular degeneration. *NPJ genomic medicine*, 5(1):34, 2020.
- [3] Daniel McDonald, Embriette Hyde, Justine W Debelius, James T Morton, Antonio Gonzalez, Gail Ackermann, Alexander A Aksenov, Bahar Behsaz, Caitriona Brennan, Yingfeng Chen, et al. American gut: an open platform for citizen science microbiome research. *Msystems*, 3(3):10–1128, 2018.
- [4] Fredrik H Karlsson, Valentina Tremaroli, Intawat Nookaew, Göran Bergström, Carl Johan Behre, Björn Fagerberg, Jens Nielsen, and Fredrik Bäckhed. Gut metagenome in european women with normal, impaired and diabetic glucose control. *Nature*, 498(7452):99–103, 2013.
- [5] Krithivasan Sankaranarayanan, Andrew T Ozga, Christina Warinner, Raul Y Tito, Alexandra J Obregon-Tito, Jiawu Xu, Patrick M Gaffney, Lori L Jervis, Derrell Cox, Lancer Stephens, et al. Gut microbiome diversity among cheyenne and arapaho individuals from western oklahoma. *Current Biology*, 25(24):3161–3169, 2015.
- [6] Anna Heintz-Buschart, Patrick May, Cédric C Laczny, Laura A Lebrun, Camille Bellora, Abhimanyu Krishna, Linda Wampach, Jochen G Schneider, Angela Hogan, Carine De Beaufort, et al. Integrated multi-omics of the human gut microbiome in a case study of familial type 1 diabetes. *Nature microbiology*, 2(1):1–13, 2016.
- [7] Nan Qin, Fengling Yang, Ang Li, Edi Prifti, Yanfei Chen, Li Shao, Jing Guo, Emmanuelle Le Chatelier, Jian Yao, Lingjiao Wu, et al. Alterations of the human gut microbiome in liver cirrhosis. *Nature*, 513(7516):59–64, 2014.
- [8] Rohit Loomba, Victor Seguritan, Weizhong Li, Tao Long, Niels Klitgord, Archana Bhatt, Parambir Singh Dulai, Cyrielle Caussy, Richele Bettencourt, Sarah K Highlander, et al. Gut microbiome-based metagenomic signature for non-invasive detection of advanced fibrosis in human nonalcoholic fatty liver disease. *Cell metabolism*, 30(3):607, 2019.
- [9] Qiang Feng, Suisha Liang, Huijue Jia, Andreas Stadlmayr, Longqing Tang, Zhou Lan, Dongya Zhang, Huihua Xia, Xiaoying Xu, Zhuye Jie, et al. Gut microbiome development along the colorectal adenoma–carcinoma sequence. *Nature communications*, 6(1):6528, 2015.
- [10] Jun Yu, Qiang Feng, Sunny Hei Wong, Dongya Zhang, Qiao yi Liang, Youwen Qin, Longqing Tang, Hui Zhao, Jan Stenvang, Yanli Li, et al. Metagenomic analysis of faecal microbiome as a tool towards targeted non-invasive biomarkers for colorectal cancer. *Gut*, 66(1):70–78, 2017.
- [11] Geoffrey D Hannigan, Melissa B Duhaime, Mack T Ruffin IV, Charlie C Koumpouras, and Patrick D Schloss. Diagnostic potential and interactive dynamics of the colorectal cancer virome. *MBio*, 9(6):10–1128, 2018.
- [12] Shinichi Yachida, Sayaka Mizutani, Hirotugu Shiroma, Satoshi Shiba, Takeshi Nakajima, Taku Sakamoto, Hikaru Watanabe, Keigo Masuda, Yuichiro Nishimoto, Masaru Kubo, et al. Metagenomic and metabolomic analyses reveal distinct stage-specific phenotypes of the gut microbiota in colorectal cancer. *Nature medicine*, 25(6):968–976, 2019.
- [13] Naoyoshi Nagata, Suguru Nishijima, Yasushi Kojima, Yuya Hisada, Koh Imbe, Tohru Miyoshi-Akiyama, Wataru Suda, Moto Kimura, Ryo Aoki, Katsunori Sekine, et al. Metagenomic identification of microbial signatures predicting pancreatic cancer from a multinational study. *Gastroenterology*, 163(1):222–238, 2022.
- [14] Eduardo Castro-Nallar, Matthew L Bendall, Marcos Pérez-Losada, Sarven Sabuncyan, Emily G Severance, Faith B Dickerson, Jennifer R Schroeder, Robert H Yolken, and Keith A Crandall. Composition, taxonomy and functional diversity of the oropharynx microbiome in individuals with schizophrenia and controls. *PeerJ*, 3:e1140, 2015.
- [15] Dorottya Nagy-Szakal, Brent L Williams, Nischay Mishra, Xiaoyu Che, Bohyun Lee, Lucinda Bateman, Nancy G Klimas, Anthony L Komaroff, Susan Levine, Jose G Montoya, et al. Fecal metagenomic profiles in subgroups of patients with myalgic encephalomyelitis/chronic fatigue syndrome. *Microbiome*, 5(1):1–17, 2017.
- [16] Yiwei Qian, Xiaodong Yang, Shaoqing Xu, Pei Huang, Binyin Li, Juanjuan Du, Yixi He, Binghua Su, Li-Ming Xu, Liang Wang, et al. Gut metagenomics-derived genes as potential biomarkers of parkinson’s disease. *Brain*, 143(8):2474–2489, 2020.
- [17] Feng Zhu, Yanmei Ju, Wei Wang, Qi Wang, Ruijin Guo, Qingyan Ma, Qiang Sun, Yajuan Fan, Yuying Xie, Zai Yang, et al. Metagenome-wide association of gut microbiome features for schizophrenia. *Nature communications*, 11(1):1612, 2020.
- [18] Sungyang Jo, Woorim Kang, Yun Su Hwang, Seung Hyun Lee, Kye Won Park, Mi Sun Kim, Hyunna Lee, Hyung Jeong Yoon, Yoo Kyoung Park, Mauricio Chalita, et al. Oral and gut dysbiosis leads to functional alterations in parkinson’s disease. *npj Parkinson’s Disease*, 8(1):87, 2022.
- [19] Christoph Laske, Stephan Müller, Oliver Preische, Victoria Ruschil, Matthias HJ Munk, Iris Honold, Silke Peter, Ulrich Schoppmeier, and Matthias Willmann. Signature of alzheimer’s disease in intestinal microbiome: results from the alzbium study. *Frontiers in Neuroscience*, 16:792996, 2022.
- [20] Zachary D Wallen, Ayse Demirkan, Guy Twa, Gwendolyn Cohen, Marissa N Dean, David G Standaert, Timothy R Sampson, and Haydeh Payami. Metagenomics of parkinson’s disease implicates the gut microbiome in multiple disease mechanisms. *Nature communications*, 13(1):6958, 2022.

- [21] Lawrence A David, Ana Weil, Edward T Ryan, Stephen B Calderwood, Jason B Harris, Fahima Chowdhury, Yasmin Begum, Firdausi Qadri, Regina C LaRocque, and Peter J Turnbaugh. Gut microbial succession follows acute secretory diarrhea in humans. *MBio*, 6(3):10–1128, 2015.
- [22] Silas Kieser, Shafiqul A Sarker, Olga Sakwinska, Francis Foata, Shamima Sultana, Zeenat Khan, Shoheb Islam, Nadine Porta, Séverine Combremont, Bertrand Betrisey, et al. Bangladeshi children with acute diarrhoea show faecal microbiomes with increased streptococcus abundance, irrespective of diarrhoea aetiology. *Environmental microbiology*, 20(6):2256–2269, 2018.
- [23] Kern Rei Chng, Angeline Su Ling Tay, Chenhao Li, Amanda Hui Qi Ng, Jingjing Wang, Bani Kaur Suri, Sri Anusha Matta, Naomi McGovern, Baptiste Janela, Xuan Fei Colin C Wong, et al. Whole metagenome profiling reveals skin microbiome-dependent susceptibility to atopic dermatitis flare. *Nature microbiology*, 1(9):1–10, 2016.
- [24] Allyson L Byrd, Clay Deming, Sara KB Cassidy, Oliver J Harrison, Weng-Ian Ng, Sean Conlan, NISC Comparative Sequencing Program, Yasmine Belkaid, Julia A Segre, and Heidi H Kong. *Staphylococcus aureus* and *staphylococcus epidermidis* strain diversity underlying pediatric atopic dermatitis. *Science translational medicine*, 9(397):eaal4651, 2017.
- [25] Angeline SL Tay, Chenhao Li, Tannistha Nandi, Kern Rei Chng, Anand Kumar Andiappan, Vijaya Saradhi Mettu, Camille de Cevins, Aarthi Ravikrishnan, Charles-Antoine Dutertre, XF Colin C Wong, et al. Atopic dermatitis microbiomes stratify into ecologic dermatotypes enabling microbial virulence and disease severity. *Journal of Allergy and Clinical Immunology*, 147(4):1329–1340, 2021.
- [26] Hsin-Wen Chang, Di Yan, Rasnik Singh, Audrey Bui, Kristina Lee, Alexa Truong, Jeffrey M Milush, Ma Somsouk, and Wilson Liao. Multiomic analysis of the gut microbiome in psoriasis reveals distinct host–microbe associations. *JID Innovations*, 2(3):100115, 2022.
- [27] Caroline Vincent, Mark A Miller, Thaddeus J Edens, Sudeep Mehrotra, Ken Dewar, and Ameer R Manges. Bloom and bust: intestinal microbiota dynamics in response to hospital exposures and *clostridium difficile* colonization or infection. *Microbiome*, 4:1–11, 2016.
- [28] Bruce A Rosa, Taniawati Supali, Lincoln Gankpala, Yenny Djuardi, Erliyani Sartono, Yanjiao Zhou, Kerstin Fischer, John Martin, Rahul Tyagi, Fatorma K Bolay, et al. Differential human gut microbiome assemblages during soil-transmitted helminth infections in indonesia and liberia. *Microbiome*, 6(1):1–19, 2018.
- [29] Meagan A Rubel, Arwa Abbas, Louis J Taylor, Andrew Connell, Ceylan Tanes, Kyle Bittinger, Valentine N Ndze, Julius Y Fonsah, Eric Ngwang, André Essiane, et al. Lifestyle and the presence of helminths is associated with gut microbiome composition in cameroonians. *Genome biology*, 21(1):1–32, 2020.
- [30] Andrew Brantley Hall, Moran Yassour, Jenny Sauk, Ashley Garner, Xiaofang Jiang, Timothy Arthur, Georgia K Lagoudas, Tommi Vatanen, Nadine Fornelos, Robin Wilson, et al. A novel ruminococcus gnavus clade enriched in inflammatory bowel disease patients. *Genome medicine*, 9:1–12, 2017.
- [31] Eric A Franzosa, Alexandra Sirota-Madi, Julian Avila-Pacheco, Nadine Fornelos, Henry J Haiser, Stefan Reinker, Tommi Vatanen, A Brantley Hall, Himel Mallick, Lauren J McIver, et al. Gut microbiome structure and metabolic activity in inflammatory bowel disease. *Nature microbiology*, 4(2):293–305, 2019.
- [32] HMP Integrative. The integrative human microbiome project: dynamic analysis of microbiome-host omics profiles during periods of human health and disease. *Cell host & microbe*, 16(3):276–289, 2014.
- [33] Wenxuan Zuo, Beibei Wang, Xin Bai, Yihui Luan, Yingying Fan, Sonia Michail, and Fengzhu Sun. 16s rRNA and metagenomic shotgun sequencing data revealed consistent patterns of gut microbiome signature in pediatric ulcerative colitis. *Scientific Reports*, 12(1):6421, 2022.
- [34] Zhuye Jie, Huihua Xia, Shi-Long Zhong, Qiang Feng, Shenghui Li, Suisha Liang, Huanzi Zhong, Zhipeng Liu, Yuan Gao, Hui Zhao, et al. The gut microbiome in atherosclerotic cardiovascular disease. *Nature communications*, 8(1):845, 2017.
- [35] Jing Li, Fangqing Zhao, Yidan Wang, Junru Chen, Jie Tao, Gang Tian, Shouling Wu, Wenbin Liu, Qinghua Cui, Bin Geng, et al. Gut microbiota dysbiosis contributes to the development of hypertension. *Microbiome*, 5:1–19, 2017.
- [36] Qiulong Yan, Yifang Gu, Xiangchun Li, Wei Yang, Liqiu Jia, Changming Chen, Xiuyan Han, Yukun Huang, Lizhe Zhao, Peng Li, et al. Alterations of the gut microbiome in hypertension. *Frontiers in cellular and infection microbiology*, 7:381, 2017.
- [37] Sean P Polster, Anukriti Sharma, Ceylan Tanes, Alan T Tang, Patricia Mericko, Ying Cao, Julián Carrión-Penagos, Romuald Girard, Janne Koskimäki, Dongdong Zhang, et al. Permissive microbiome characterizes human subjects with a neurovascular disease cavernous angioma. *Nature communications*, 11(1):2659, 2020.
- [38] Zujian Xiong, Kang Peng, Shaoyu Song, Yongwei Zhu, Jia Gu, Chunhai Huang, and Xuejun Li. Cerebral intraparenchymal hemorrhage changes patients’ gut bacteria composition and function. *Frontiers in Cellular and Infection Microbiology*, 12:829491, 2022.
- [39] Josh L Espinoza, Derek M Harkins, Manolito Torralba, Andres Gomez, Sarah K Highlander, Marcus B Jones, Pamela Leong, Richard Saffery, Michelle Bockmann, Claire Kuelbs, et al. Supragingival plaque microbiome ecology and functional potential in the context of health and disease. *MBio*, 9(6):10–1128, 2018.
- [40] Paolo Ghensi, Paolo Manghi, Moreno Zolfo, Federica Armanini, Edoardo Pasolli, Mattia Bolzan, Alberto Bertelle, Federico Dell’Acqua, Ester Dellasega, Romina Waldner, et al. Strong oral plaque microbiome signatures for dental implant diseases identified by strain-resolution metagenomics. *npj Biofilms and Microbiomes*, 6(1):47, 2020.
- [41] Roland Wirth, Gergely Maróti, Lída Lipták, Mónika Mester, Alaa Al Ayoubi, Bernadett Pap, Melinda Madléna, János Minárovits, and Kornél L Kovács. Microbiomes in supragingival biofilms and saliva of adolescents with gingivitis and gingival health. *Oral Diseases*, 28(7):2000–2014, 2022.

- [42] Zi Ye, Ni Zhang, Chunyan Wu, Xinyuan Zhang, Qingfeng Wang, Xinyue Huang, Liping Du, Qingfeng Cao, Jihong Tang, Chunjiang Zhou, et al. A metagenomic study of the gut microbiome in behcet's disease. *Microbiome*, 6(1):1–13, 2018.
- [43] Qiyun Zhu, Qiangchuan Hou, Shi Huang, Qianying Ou, Dongxue Huo, Yoshiki Vázquez-Baeza, Chaoping Cen, Victor Cantu, Mehrbod Estaki, Haibo Chang, et al. Compositional and genetic alterations in graves' disease gut microbiome reveal specific diagnostic biomarkers. *The ISME journal*, 15(11):3399–3411, 2021.
- [44] Yolanda Guillén, Marc Noguera-Julian, Javier Rivera, Maria Casadellà, Alexander S Zevin, Mutsa Rocafort, Mariona Parera, Cristina Rodríguez, Marçal Arumí, Jorge Carrillo, et al. Low nadir cd4+ t-cell counts predict gut dysbiosis in hiv-1 infection. *Mucosal immunology*, 12(1):232–246, 2019.
- [45] Yongfei Hu, Yuqing Feng, Jiannan Wu, Fei Liu, Zhiguo Zhang, Yanan Hao, Shihao Liang, Boxing Li, Jing Li, Na Lv, et al. The gut microbiome signatures discriminate healthy from pulmonary tuberculosis patients. *Frontiers in cellular and infection microbiology*, 9:90, 2019.
- [46] Marie-Madlen Pust, Lutz Wiehlmann, Colin Davenport, Isa Rudolf, Anna-Maria Dittrich, and Burkhard Tümmler. The human respiratory tract microbial community structures in healthy and cystic fibrosis infants. *npj Biofilms and Microbiomes*, 6(1):61, 2020.
- [47] Tao Zuo, Fen Zhang, Grace CY Lui, Yun Kit Yeoh, Amy YL Li, Hui Zhan, Yating Wan, Arthur CK Chung, Chun Pan Cheung, Nan Chen, et al. Alterations in gut microbiota of patients with covid-19 during time of hospitalization. *Gastroenterology*, 159(3):944–955, 2020.
- [48] Xiangning Bai, Aswathy Narayanan, Magdalena Skagerberg, Rafael Ceña-Diez, Christian G Giske, Kristoffer Strålin, and Anders Sönnnerborg. Characterization of the upper respiratory bacterial microbiome in critically ill covid-19 patients. *Biomedicines*, 10(5):982, 2022.
- [49] Qin Liu, Joyce Wing Yan Mak, Qi Su, Yun Kit Yeoh, Grace Chung-Yan Lui, Susanna So Shan Ng, Fen Zhang, Amy YL Li, Wenqi Lu, David Shu-Cheong Hui, et al. Gut microbiota dynamics in a prospective cohort of patients with post-acute covid-19 syndrome. *Gut*, 71(3):544–552, 2022.
- [50] Guohui Xiao, Zhao Cai, Qinglong Guo, Taosheng Ye, Yimin Tang, Peikun Guan, Juanjuan Zhang, Min Ou, Xiangdong Fu, Lili Ren, et al. Insights into the unique lung microbiota profile of pulmonary tuberculosis patients using metagenomic next-generation sequencing. *Microbiology Spectrum*, 10(1):e01901–21, 2022.
- [51] Fen Zhang, Yating Wan, Tao Zuo, Yun Kit Yeoh, Qin Liu, Lin Zhang, Hui Zhan, Wenqi Lu, Wenye Xu, Grace CY Lui, et al. Prolonged impairment of short-chain fatty acid and l-isoleucine biosynthesis in gut microbiome in patients with covid-19. *Gastroenterology*, 162(2):548–561, 2022.
- [52] Tuoyu Zhou, Jingyuan Wu, Yufei Zeng, Junfeng Li, Jun Yan, Wenbo Meng, Huawen Han, Fengya Feng, Jufang He, Shuai Zhao, et al. Sars-cov-2 triggered oxidative stress and abnormal energy metabolism in gut microbiota. *MedComm*, 3(1):e112, 2022.
- [53] Otoniel Maya-Lucas, Selvasankar Murugesan, Khemlal Nirmalkar, Luis David Alcaraz, Carlos Hoyo-Vadillo, María Luisa Pizano-Zárate, and Jaime García-Mena. The gut microbiome of mexican children affected by obesity. *Anaerobe*, 55:11–23, 2019.
- [54] Xinyu Qi, Chuyu Yun, Lulu Sun, Jialin Xia, Qing Wu, Ying Wang, Lina Wang, Yangming Zhang, Xianyi Liang, Liying Wang, et al. Gut microbiota–bile acid–interleukin-22 axis orchestrates polycystic ovary syndrome. *Nature medicine*, 25(8):1225–1233, 2019.
- [55] Sankhya Bommana, Gracie Richards, Mike Kama, Reshma Kodimerla, Kenan Jijakli, Timothy D Read, and Deborah Dean. Metagenomic shotgun sequencing of endocervical, vaginal, and rectal samples among fijian women with and without chlamydia trachomatis reveals disparate microbial populations and function across anatomic sites: a pilot study. *Microbiology spectrum*, 10(3):e00105–22, 2022.
- [56] Zheng Sun, Meng Zhang, Min Li, Yogendra Bhaskar, Jinshan Zhao, Youran Ji, Hongbing Cui, Heping Zhang, and Zhihong Sun. Interactions between human gut microbiome dynamics and sub-optimal health symptoms during seafaring expeditions. *Microbiology Spectrum*, 10(1):e00925–21, 2022.
- [57] David M Blei, Alp Kucukelbir, and Jon D McAuliffe. Variational inference: A review for statisticians. *Journal of the American statistical Association*, 112(518):859–877, 2017.